Pressure Waves in Soils Using a Split–Hopkinson Pressure Bar

C. ALLEN ROSS
PHILLIP T. NASH
GERARD J. FRIESENHAHN

SOUTHWEST RESEARCH INSTITUTE
P.O. DRAWER 28510
SAN ANTONIO, TEXAS 78284

JULY 1986

FINAL REPORT

DTIC
ELECTE
SEP 1 8 1986
S D
D

APRIL 1984 - FEBRUARY 1986

APPROVED FOR PUBLIC RELEASE: DISTRIBUTION UNLIMITED

AD-A172 080

DTIC FILE COPY

ENGINEERING & SERVICES LABORATORY
AIR FORCE ENGINEERING & SERVICES CENTER
TYNDALL AIR FORCE BASE, FLORIDA 32403

86 9 17 04

NOTICE

SECURITY CLASSIFICATION OF THIS PAGE (When Data Entered)

REPORT DOCUMENTATION PAGE	READ INSTRUCTIONS BEFORE COMPLETING FORM

1. REPORT NUMBER	2. GOVT ACCESSION NO.	3. RECIPIENT'S CATALOG NUMBER
ESL-TR-86-29	AD-A191208	

4. TITLE (and Subtitle)	5. TYPE OF REPORT & PERIOD COVERED
Pressure Waves in Soils Using a Split-Hopkinson Pressure Bar	Final Report April 1984-Feb 1986
	6. PERFORMING ORG. REPORT NUMBER

7. AUTHOR(s)	8. CONTRACT OR GRANT NUMBER(s)
C. Allen Ross Phillip T. Nash Gerard J. Friesenhahn	F08635-84-K-0153

9. PERFORMING ORGANIZATION NAME AND ADDRESS	10. PROGRAM ELEMENT, PROJECT, TASK AREA & WORK UNIT NUMBERS
Southwest Research Institute P.O. Drawer 28510 San Antonio, Texas 78284	

11. CONTROLLING OFFICE NAME AND ADDRESS	12. REPORT DATE
Air Force Engineering and Services Center Tyndall AFB, Florida 32403	July 1986
	13. NUMBER OF PAGES

14. MONITORING AGENCY NAME & ADDRESS(If different from Controlling Office)	15. SECURITY CLASS. (of this report)
	UNCLASSIFIED
	15a. DECLASSIFICATION/DOWNGRADING SCHEDULE

16. DISTRIBUTION STATEMENT (of this Report)

Approved for public release; distribution unlimited.

17. DISTRIBUTION STATEMENT (of the abstract entered in Block 20, if different from Report)

18. SUPPLEMENTARY NOTES

19. KEY WORDS (Continue on reverse side if necessary and identify by block number)

Hopkinson Bar	Wave Reflection
Soils	Wave Refraction
Pressure Waves	Soil Damping
Wave Propagation	Attenuation
Critical Incidence Angle	

20. ABSTRACT (Continue on reverse side if necessary and identify by block number)

Soil specimen lengths of 2.0, 4.0 and 6.0 inches were tested in a split-Hopkinson pressure bar (SHPB) to determine effects of grain size, moisture content, confining pressure, and specimen length on material damping, wave speed and transmissibility.

For these SHPB tests the soil specimen length was long compared to the pulse length of the loading pulse. Three different grain sizes were tested for determination of damping/attenuation coefficients. A medium to fine sandy

DD FORM 1473 1 JAN 71   EDITION OF 1 NOV 68 IS OBSOLETE

SECURITY CLASSIFICATION OF THIS PAGE (When Data Entered)

soil was tested both statically and dynamically for effects of moisture content, and compaction energy. The main conclusion is that the split-Hopkinson pressure bar can be used to obtain meaningful data on soil properties at intermediate strain rates. Considerable scatter is also present in the laboratory data. If further soil tests at intermediate strain rates are desired then the SHPB should be modified to accommodate a triaxial test cell.
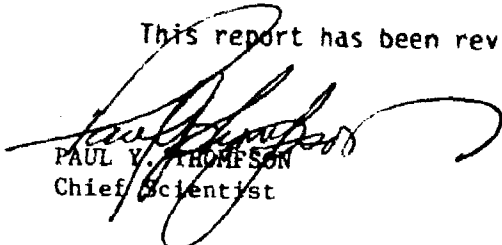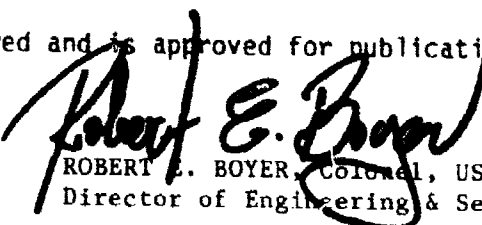
PREFACE

This report was prepared by the Department of Energetic Systems, Southwest Research Institute, San Antonio, Texas, under Contract No. F08635-84-K-0153 for Headquarters, Air Force Engineering and Services Center, Engineering and Services Laboratory (AFESC/RDC), Tyndall AFB, Florida.

This report summarizes the results of work to investigate the feasibility of testing soil specimens in a split-Hopkinson pressure bar. The work was initiated in April 1984 and completed in February 1986. Mr. P. T. Nash served as project officer for Southwest Research Institute and Dr. P. Y. Thompson served as the project officer for AFESC/RD. Dr. C. A. Ross of Ross Engineering Association Inc., served as a consultant for this investigation.

This report has been reviewed by the Public Affairs Office (PA) and is releasable to the National Technical Information Service (NTIS). At NTIS, it will be available to the general public, including foreign nationals.

This report has been reviewed and is approved for publication.

PAUL Y. THOMPSON
Chief Scientist

ROBERT L. BOYER, Colonel, USAF
Director of Engineering & Services Laboratory

Accesion For	
NTIS CRA&I	☑
DTIC TAB	☐
Unannounced	☐
Justification	
By	
Distribution /	
Availability Codes	
Dist	Avail and / or Special
A-1	

i

(The reverse of this page is blank.)

TABLE OF CONTENTS

Section I   Title

TABLE OF CONTENTS (CONTINUED)

TABLE OF CONTENTS (CONCLUDED)

APPENDIX	Title	Page

LIST OF FIGURES

LIST OF TABLES

SECTION I

INTRODUCTION

A.   OBJECTIVE

The major objective of the research effort was to determine the
feasibility of soil testing in a split-Hopkinson pressure (SHPB) and evaluate
the data to determine their applicability to modification of existing predictive
techniques for pressure waves in soils. In addition, a cursory examination of
the "total reflection" phenomenon was to be undertaken.

B.   BACKGROUND

1. Pressure Waves in Soils

Pressure waves generated by underground explosions of a known weight
propagate radially from the explosive source and generally the peak pressure
magnitude P, particle velocity v, arrival time t_a, pulse length τ, and rise
time t_r are measured using a soil gauge stationed at some distance R. If the
soil gauge is positioned so that the measuring face is normal to a radial line
from the source to the gauge, and the gauge is free to move with the soil
particles, then the pressure pulse is called a free-field pressure. When the
gauge is rotated so that the measuring face is parallel to a radial line from
the source to the gauge, and the gauge is free to move with the wave, the
pressure pulse is called a side-on pressure. If the gauge is embedded in a
rather massive or rigid structure which does not move relative to the particle
motion, then the pressure is called a reflected pressure. Usually, the term,
reflected pressure, is reserved for the pressure when measured normal to the
wave particle motion; however, reflected pressures at other than normal
incidence are also called reflected pressures to distinguish them from the
free-field pressures which are always measured normal to the particle motion.

In elementary wave mechanics, the pressures or stresses associated
with pressure wave motion are given names relative to an interface between two
media. If a pressure wave is traveling in Medium 1 and impinges on an

1

interface separating Medium 1 and Medium 2, the various waves are denoted as the incident wave, the reflected wave, and the transmitted or diffracted wave. The incident wave traveling in Medium 1, is comparable to the free-field wave discussed above. When the incident wave impinges on the interface, a wave(s) is reflected and propagates back into Medium 1 and transmitted or diffracted waves propagate into Medium 2. The transmitted wave is then comparable to the soil reflected wave described above. Usually, the wave reflected back into the soil from a rigid structure is not measured. The mechanics of wave motion will be discussed later, but a soil-reflected pressure measured on a relatively rigid body will be assumed to be the same as the transmitted or refracted pressure propagated in that body.

Pressures measured in soil show very large scatter in the data. An example of such scatter is given in Reference 1 in terms of a standard deviation of 0.875 for the natural log (base e) of pressure. This means that the scatter or standard deviation for a given pressure would be from 2.4 times that pressure at the upper limit to 0.42 times that pressure for a lower limit or an approximate variation in pressure of approximately ± 70 percent. This scatter is given for pressures ranging from approximately 10,000 psi to a few psi. Data reported by the National Defense Research Committee (NDRC) (Reference 2) show a scatter of approximately ± 25 percent for pressures ranging from 500 - 5 psi. Peak particle velocity varies approximately ±50 percent for a combination of several sets of data given in Reference 3. Ground-induced particle velocities from a nuclear or simulated nuclear explosion, as given in Reference 4, show variation as much as 2.5-5.0 orders of magnitude. Various particle velocity and seismic velocity predictive equations were examined in Reference 5. Comparisons of the various predictions show that variations as high as factors of 10-50 may exist between one equation and another. It is with the large scatter and variations of these parameters in mind that the experimental research, associated with soil samples in a split-Hopkinson pressure bar (SHPB), was initiated.

A split-Hopkinson pressure bar (SHPB), described in some detail in Appendix, A has been used traditionally to examine strain rate effects on properties of solid materials. Referring to Figure 1, a short impactor or striker bar of velocity v is impacted against a longer incident bar which

2
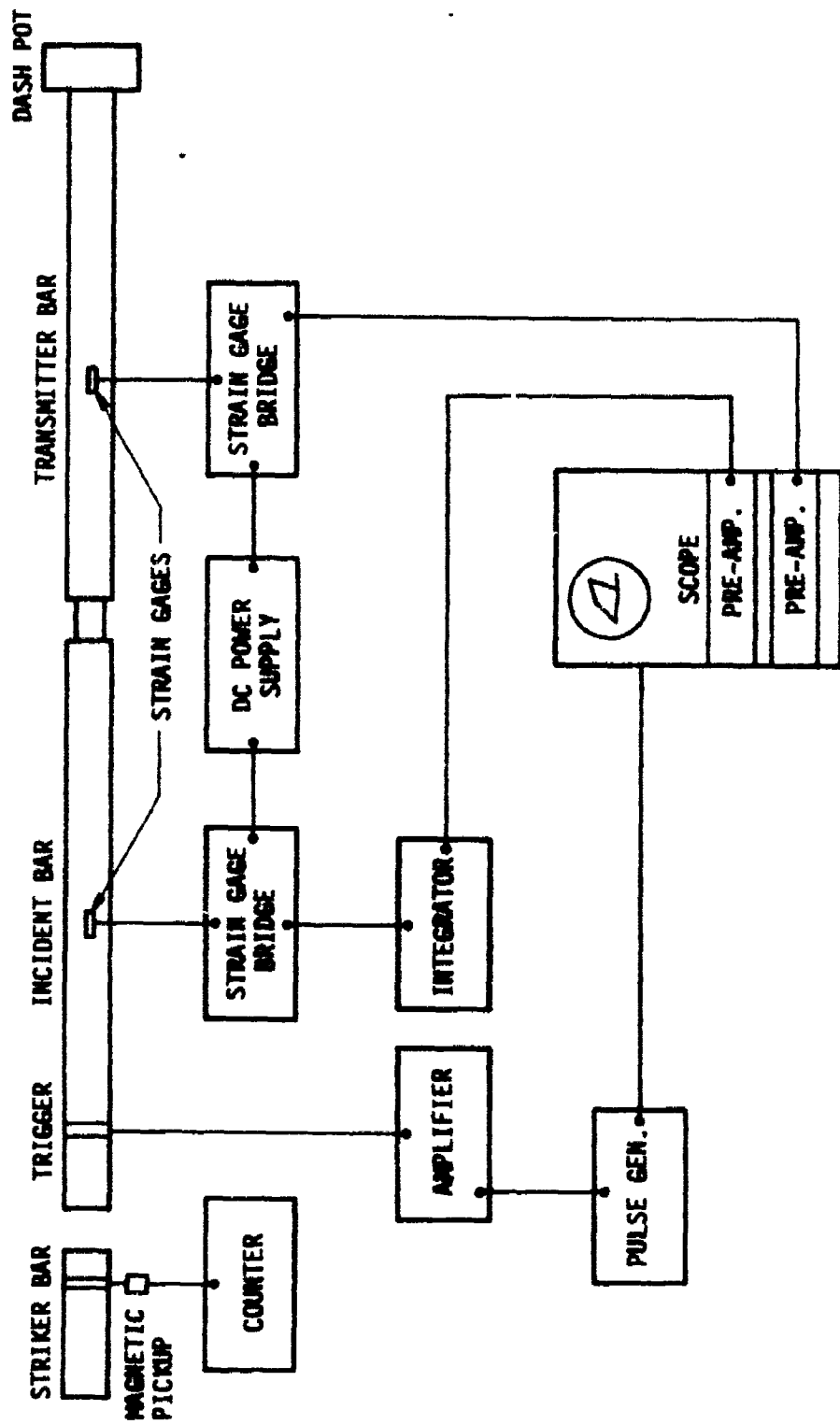
Figure 1. Schematic of Split-Hopkinson Pressure Bar

results in a stress wave propagating in opposite directions in each bar. The length of the striker bar determines the length of the pressure pulse and the impact velocity determines the peak pressure magnitude. The pressure pulse impinges on a specimen sandwiched between the incident bar and the transmitter bar. At the specimen, a part of the pulse is transmitted into the transmitter bar and part of the pulse is reflected back into the incident bar. The transmitted pulse is proportional to the stress in the specimen and the time integral of the reflected pulse is proportional to the strain in the specimen. Normally the pulse strain signatures are measured at equal distances from the specimen which make them coincident in time, and may be displayed as a dynamic stress-strain curve. If the dynamic stress-strain curve is the prime objective of the tests described above, the specimen length must be short enough so that many reflections occur within the specimen while it is being loaded by the incident pulse. These multiple reflections will insure that the specimen is under a uniform stress condition over the length of the specimen.

The research study reported here used a variation of the above decribed SHPB and a combination of specimen length and striker bar length to insure that only a single pulse may be recorded during the pulse traverse of the specimen. In this case, a known pulse length and shape could be used to study effects of changes in soil particle size, moisture content, confining pressure, and density. Furthermore, the diameter of the bar was made large enough to accommodate a typical piezoelectric pressure gauge for comparison with data from SHPB measurements. The final SHPB design described later could be used to obtain stress-strain curves of soil samples, similar to those reported in Reference 6; however, this was not the objective of this study. This study is restricted to the study of long soil specimens with short pressure pulses passing through them.

2. Compressional Wave at Critical Incidence

A short discussion of elementary wave mechanics is given in Appendix B. Stated simply, the basic physical phenomena are that when either compressional or distortional waves traveling in Medium 1 impinges on an interface between that Medium and Medium 2, generally distortional waves and

4

compressional waves are both reflected into Medium 1 and refracted into Medium 2. The relative peak magnitudes, propagation directions and energy content of the reflected and refracted waves are dependent on the incident angle at the interface and the density and wave speed of the two media. When either wave speed of Medium 1 is less than the corresponding wave speed of Medium 2, a critical incidence angle exists for that type of wave. This critical incidence angle is evidenced by a refracted angle of 90 degrees, and, since the refracted angle cannot physically be greater than 90 degrees, then complete refraction or transmission does not occur and the phenomenon is termed "total reflection." The use of this phenomenon is in the study of seismic layering and is described in many texts such as Reference 7.

In the study of pressure waves traveling in soil which impinge on buried structures one discovers that the ratio of wave speeds of many soils to that of concrete material is approximately 0.1 or 0.2. This means that the critical incidence angle then may be as low as 10 to 20 degrees for a soil/concrete interface. Then for a very close-in underground explosion against a concrete wall total reflection may exist for the major portion of the wall. The major concern here is what portion of the energy of the pressure wave is transmitted to the refracting medium. This required closer examination of the total reflection phenomenon relative to compressional pressure waves impinging on nonnormal interfaces.

C. SCOPE/APPROACH

The research effort discussed in this report is broken into two parts, (1) pressure waves in soils and, (2) compressional waves at critical incidence. Part 1, pressure waves in soils, was the major part of the research and was totally experimental. Part 2 comprised only about 15 percent of the total research effort and was analytical in nature. In the report the two parts are discussed in separate sections or subsections.

5

SECTION II

SPLIT-HOPKINSON PRESSURE BAR DESIGN

A. INTRODUCTION

1. General Considerations

As mentioned in Section I-A.2, the SHPB would be designed so as to accommodate a long soil sample relative to a striker bar length. The other main consideration is that the bar material be of as high a yield strength as possible with a low characteristic impedance (product of material wave speed and density). Rod materials are limited which are readily available in lengths required to accommodate the long soil sample and its inherent low wave propagation speed. Proper lengths of special materials which might prove useful require special orders and long lead times for delivery. The basic materials of reasonable availability were steel and aluminum. The characteristic impedance of aluminum is approximately 60 percent of that of steel. However, the highest compressive strength of aluminum material is only about 27 percent of that of available high-strength steel. The advantage of using steel over aluminum is also present in bar stiffness and hardness. For these and the other reasons discussed, steel was selected as a bar material.

The final decision on bar stock for the SPHB design was determined by availability. The proper lengths of 2-inch diameter stainless steel PH 13-8 Mo rods were located and purchased from Advanced Alloys, Inc., 128 Adams, Hauppauge, N.Y., 11787. Heat treatment, straightening, material certification, and shipping of the bars were handled by Advance Alloys, Inc. All bars for the Southwest Research Institute (SwRI) SHPB system were fabricated from the PH 13-8 Mo stainless steel rods.

2. Gas Gun Launcher

Several SHPB systems are designed using a large cam and torsional bar to launch the striker bar against the incident bar. Probably, the safest and most reliable is a simple compressed air or gas gun with a quick-acting

6

pressure relief piston. The design chosen here is based on a gas gun system discussed in Reference 8 and is shown schematically in Figure 2. One disadvantage is that the projectile must be muzzle-loaded, but this is accomplished easily, using a flexible rod. Venting of the barrel was incorporated to prevent multiple impacts of the striker bar.

The principles of operation of the system are:

a. The striker bar is positioned in the barrel.
b. The cylinder containing the inner piston is pressurized to approximately one-third the desired operating pressure. This positions the inner piston against the front face of the pressure chamber and seals the pressure chamber against leakage into the barrel.
c. The pressure chamber is adjusted to the desired pressure.
d. The pressure in the inner cylinder is dumped by the pneumatic valve, the inner piston moves rearward, and the gas pressure enters the barrel and exerts against the end of striker bar.

The gas gun system was designed to launch long striker bars, therefore requiring reasonably high pressures, and, if required, may be used as a stand-alone, high-velocity, gas gun. A design load of 2000 psi (13.8 MPa) and a material yield stress of 30,000 psi (205.9 MPa) were used in the design of the outer cylinder and flanges of the SwRI gas gun launcher. This design meets the specifications required by the ASME Boiler and Pressure Vessel Code (Reference 9).

An estimate of velocity and incident bar stress may be calculated using a reversible adiabatic expansion of the gas in the pressure chamber into the gun barrel. This estimate assumes frictionless sliding of the striker bar and that the work done in expanding the gas is converted to kinetic energy of the striker bar. Using the above assumptions, the velocity of a 2-inch diameter steel striker bar driven by nitrogen is given by

$$
u_{sb} = 46.4 \left(\frac{P_{pc}}{V_{sb}} \right)^{\frac{1}{2}} \left\{ - V_{pc} \left[\left(\frac{V_{pc}}{V_{pc} + V_b} \right)^{0.4} - 1 \right] \right\}^{\frac{1}{2}}
$$

(1)

7
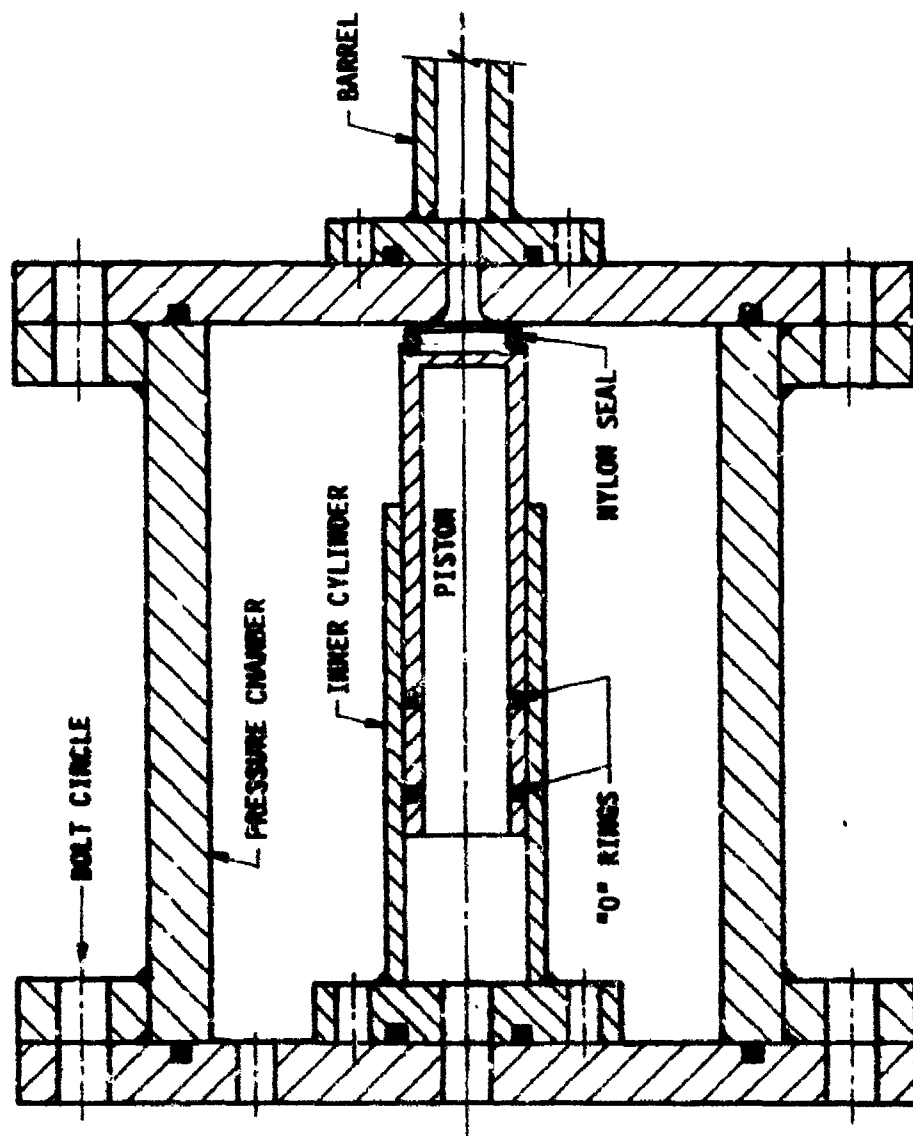
Figure 2. Schematic of Gas Gun Launcher.

BARREL

BOLT CIRCLE

PRESSURE CHAMBER

INNER CYLINDER

PISTON

NYLON SEAL

"O" RINGS

where $\quad v_{sb}$ = striker bar velocity, in/sec,

P_{pc} = gauge pressure of pressure chamber, psi,

L_{sb} = length of striker bar, in,

V_{pc} = volume of pressure chamber, in^3,

V_b = effective barrel volume, in^3.

From Appendix A, the incident stress resulting from an impact of a steel striker bar against a steel bar of same diameter is given as

$$\sigma_I = 72.2 \ v_{sb} \tag{2}$$

where $\quad \sigma_I$ = peak stress in incident bar, psi
v_{sb} = striker bar velocity, in/sec.

A combination of Equations (1) and (2) results in an estimate of the incident bar stress in terms of volumes and pressures of the gas gun system. Metric equivalents are omitted for the units of measure because the numerical constant of each equation is related to the units given for each term. A sketch of the final design showing the basic dimensions is given in Figures 3 and 4.

3. Final Design of SwRI SHPB System

After one decides the SHPB bar material and diameter, the final bar length and support system are dictated by strain gauge placement and specimen location. For conventional SHPB operation, the length of the incident and transmitter bars must be approximately 10 inches greater than twice the length of the striker bar to avoid problems of overlapping of the incident and reflected strain signals in the incident bar and transmitter bar. Elongation of the transmitted pulse in soil samples is caused by the dispersive nature of

9

Figure 3. Sketch of Final Design for Gas Gun Launcher.
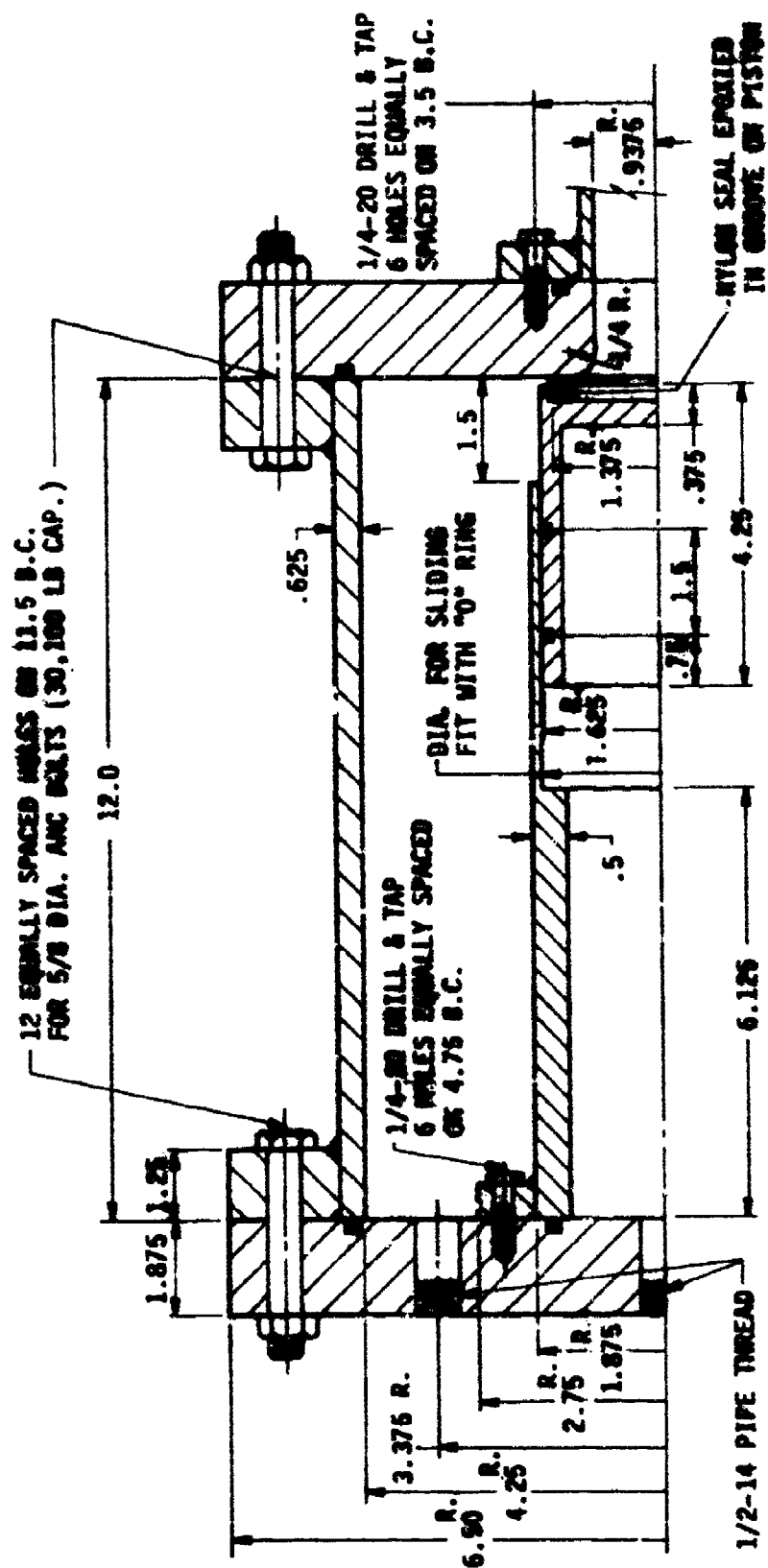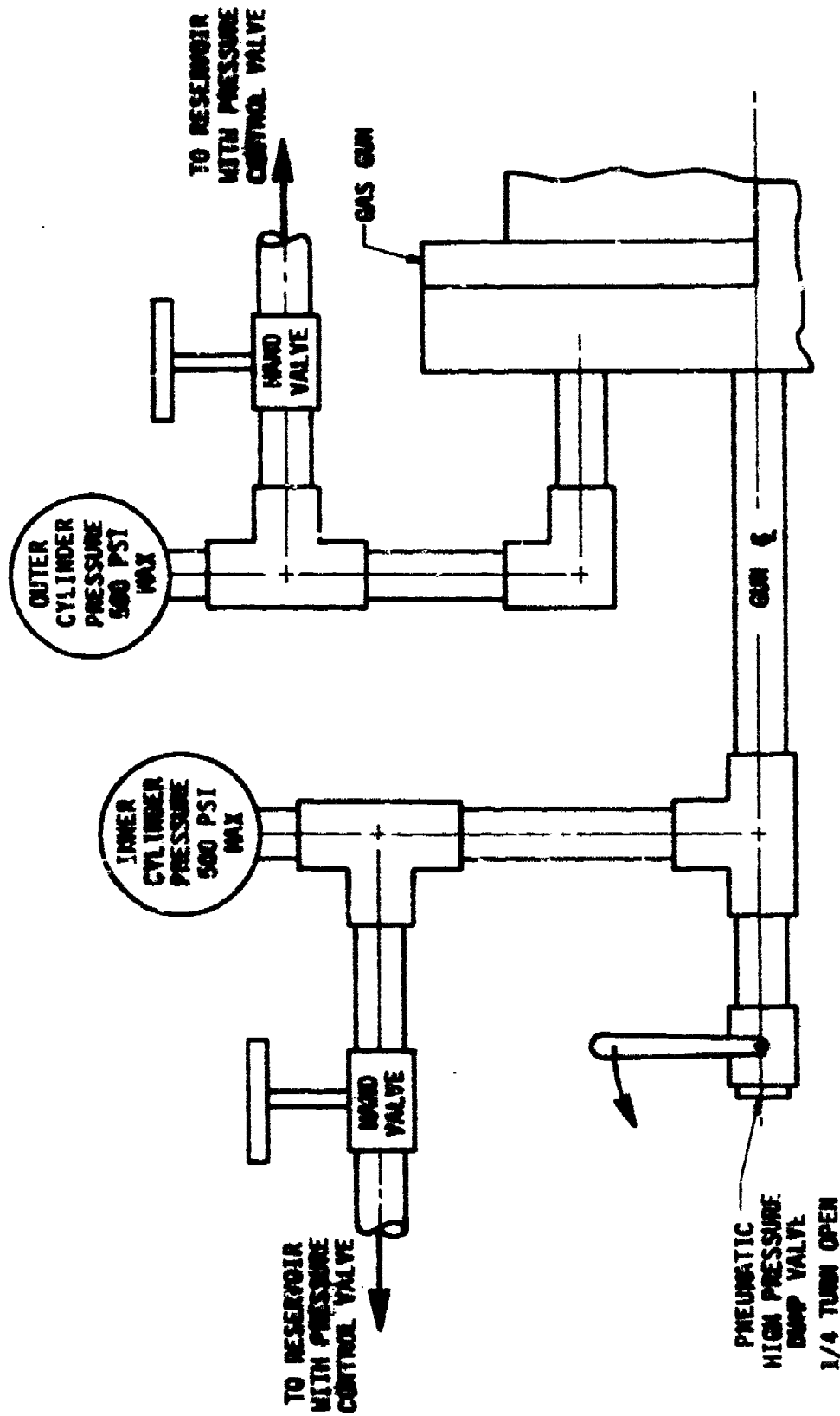
Figure 4. Sketch of Plumbing for Gas Gun Launcher.

11

the soil material, and, for the SwRI SHPB, these bars were made relatively long. The final dimensions of the bars are given in Table 1. A sketch of the final overall design is given in Figure 5.

TABLE 1. MAJOR BAR DIMENSIONS FOR SWRI SHPB SYSTEM

Bar	Length
Incident	12.0 ft, (144.0 in), (3.66 m)
Transmitter	11.0 ft, (132.0 in), (3.35 m)
Throw-off	5.0 ft, (60 in), (1.52 m)
Striker (three lengths)	4.0 in (10.16 cm)
	8.0 in (20.32 cm)
	16.0 in (40.64 cm)

All bar diameters 2.0 in (5.08 cm), PH 13-8 Mo stainless

B.   SOUTHWEST RESEARCH INSTITUTE SPLIT-HOPKINSON PRESSURE BAR (SwRI SHPB)

1.   Overall SwRI SHPB System

Based on the material availability for bar material, the SwRI SHPB final design placed the bar lengths of Table 1 on a foundation and set of supports as shown in Figure 5. The support system on the deep I-beam consists of journal bearings spaced about 3 feet (0.92 meters) apart with the center-line of the bars 7.5 inches (19.05 cm) above the top of the deep I-beam. This gives a bar height of approximately 4 feet from the floor.
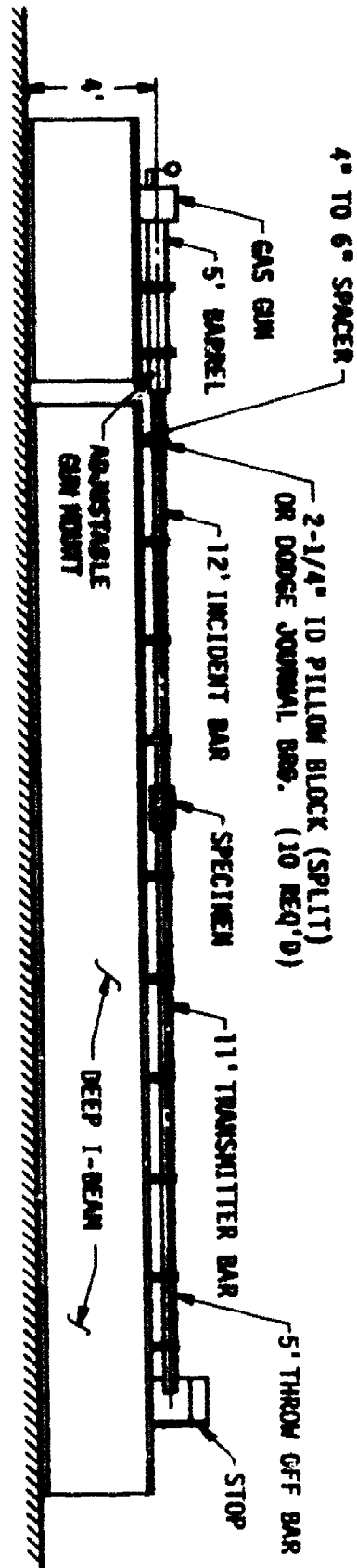
Figure 5. Schematic of 2-inch Diameter Split-Hopkinson Pressure Bar.

2. Soil Specimen Holder

Ideally the soil specimen should be held in a container whose stiffness would prevent only lateral motion. This results in a plane strain condition when axial loads are applied. For the soil specimen holder, a 12-inch (30.5 cm) long steel tube of 2 inches (5.08 cm) ID and 4 inches (10.16 cm) OD was chosen. The weight of the steel tube is a disadvantage in specimen preparation, but does satisfy the condition of plane strain during the test. No internal surface preparation, except for the final internal machining, was accomplished. Friction plays a part in the results, but all tests were conducted in the same specimen holder. The specimen holder was positioned in the bar shown in Figure 6.

In placing the soil specimen in the specimen holder, it was necessary to contain the soil at both ends of the specimen, as shown in Figure 6. The initial containment was to place the pressure gauge holder in one end of the specimen holder, put in desired amount of soil and then slip in a slightly oversize steel shim at the other end of the specimen. This configuration is shown schematically in Figure 6. Many tests were conducted using this configuration; however, leakage of soil during dry soil test and water during moist soil test led to a modification as shown in Figure 7. Here, the pressure gauge holder, without the pressure gauge, was used as a spacer and a thin steel wafer with an "O" ring was placed at each end of the soil specimen. This proved to be very effective in preventing leakage from each end of the specimen. Tests were performed without soil specimens and no discernible differences were observed between pressure-pulse transmission with and without the wafers.

3. Pressure Gauge Holder

If a pressure gauge or transducer is placed at the end of the soil sample, access for electrical loads must be available. This was accomplished for a PCB® quartz pressure transducer, used previously in work reported in Reference 1. A sketch of the pressure gauge holder is shown in Figure 8.

14
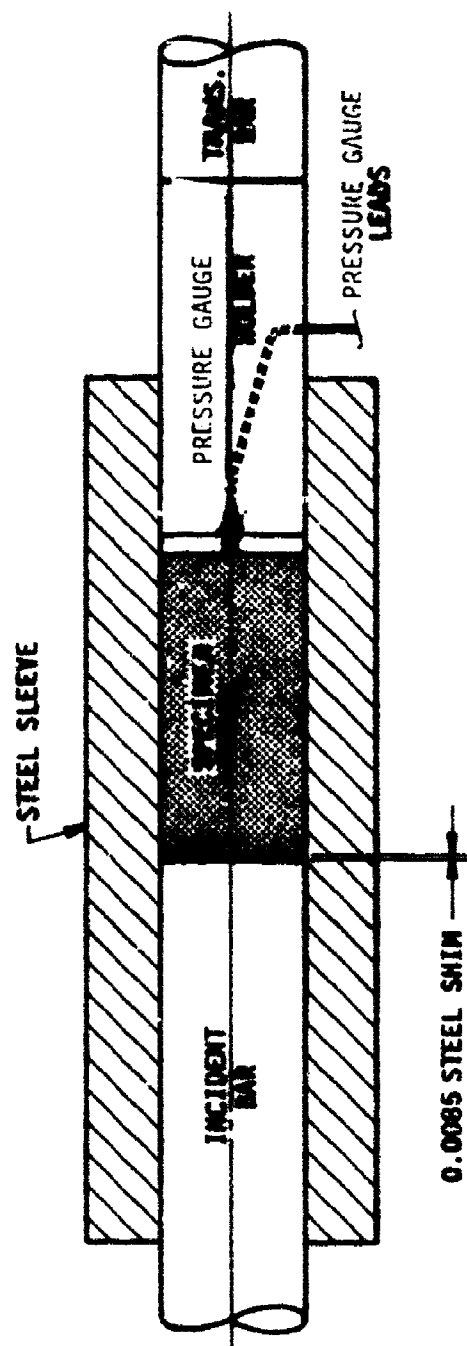
Figure 6. Sketch of Specimen Holder with Steel Shim and Pressure Gauge Holder

15
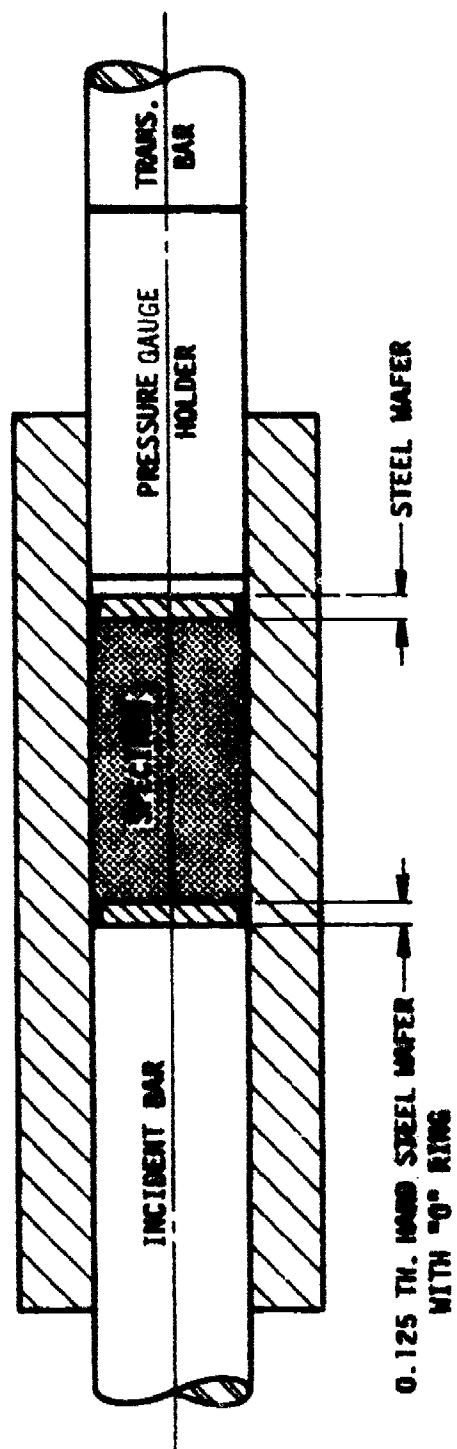
Figure 7. Sketch of Specimen Holder with Steel Wafers Installed.

16
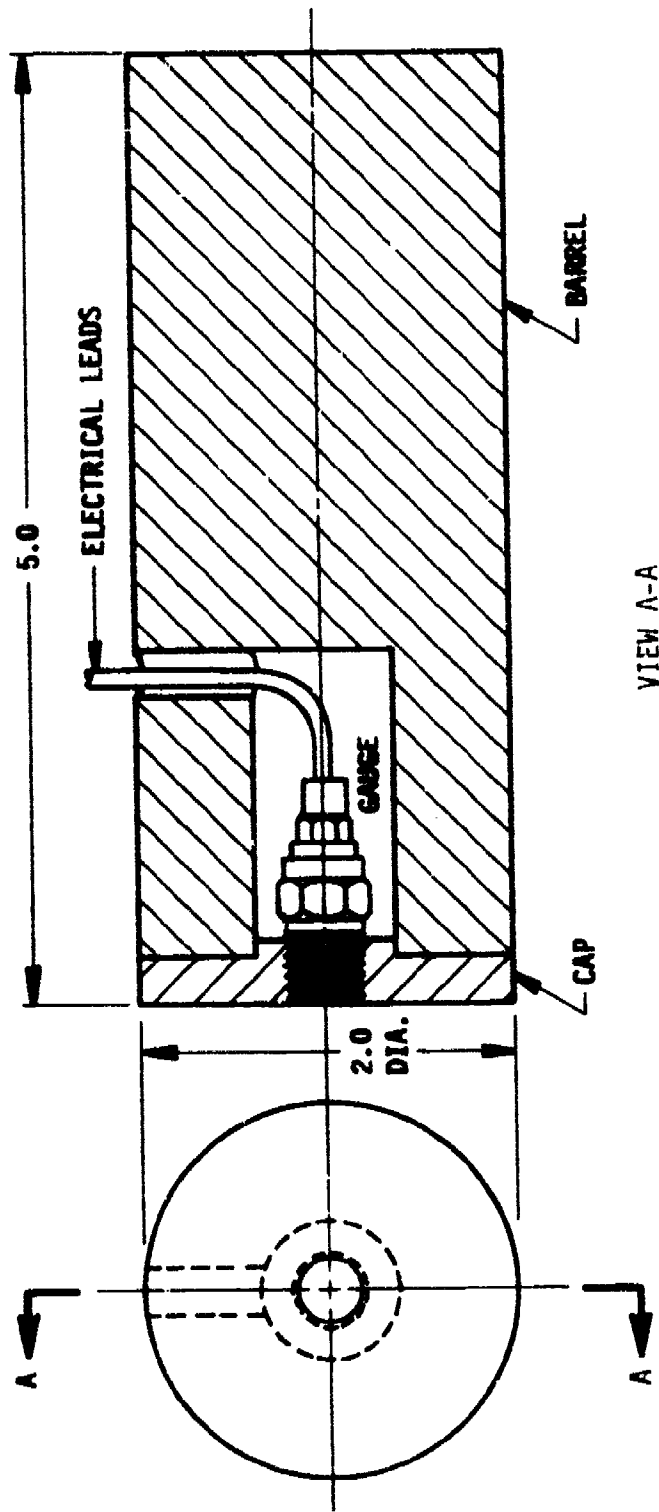
Figure 8. Sketch of Pressure Gauge Holder.

VIEW A-A

Tests were conducted with and without the pressure gauge holder to determine the effects of the discontinuities in the holder on the wave transmission. No discernible differences were experienced in these tests. The pressure gauge holder was positioned in the specimen, as shown in Figures 6 and 7, with the face of the pressure gauge approximately 2.5 inches from the end of the specimen holder.

When the steel wafers were used in the final series of tests, the pressure gauge holder was simply used as a spacer. Future tests using the pressure gauge would require modification of the gauge plate of the holder, so that an "O" ring could be used.

4. Electronic Data Recording System

Strain of the various pressure pluses was monitored using strain gauges attached to the incident bar and at two places on the transmitter bar. The pressure at the end of the soil specimen was monitored in many of the tests using a quartz pressure transducer. A schematic of the electronic system is shown in Figure 9. The various items shown in Figure 9 are listed in Table 2.
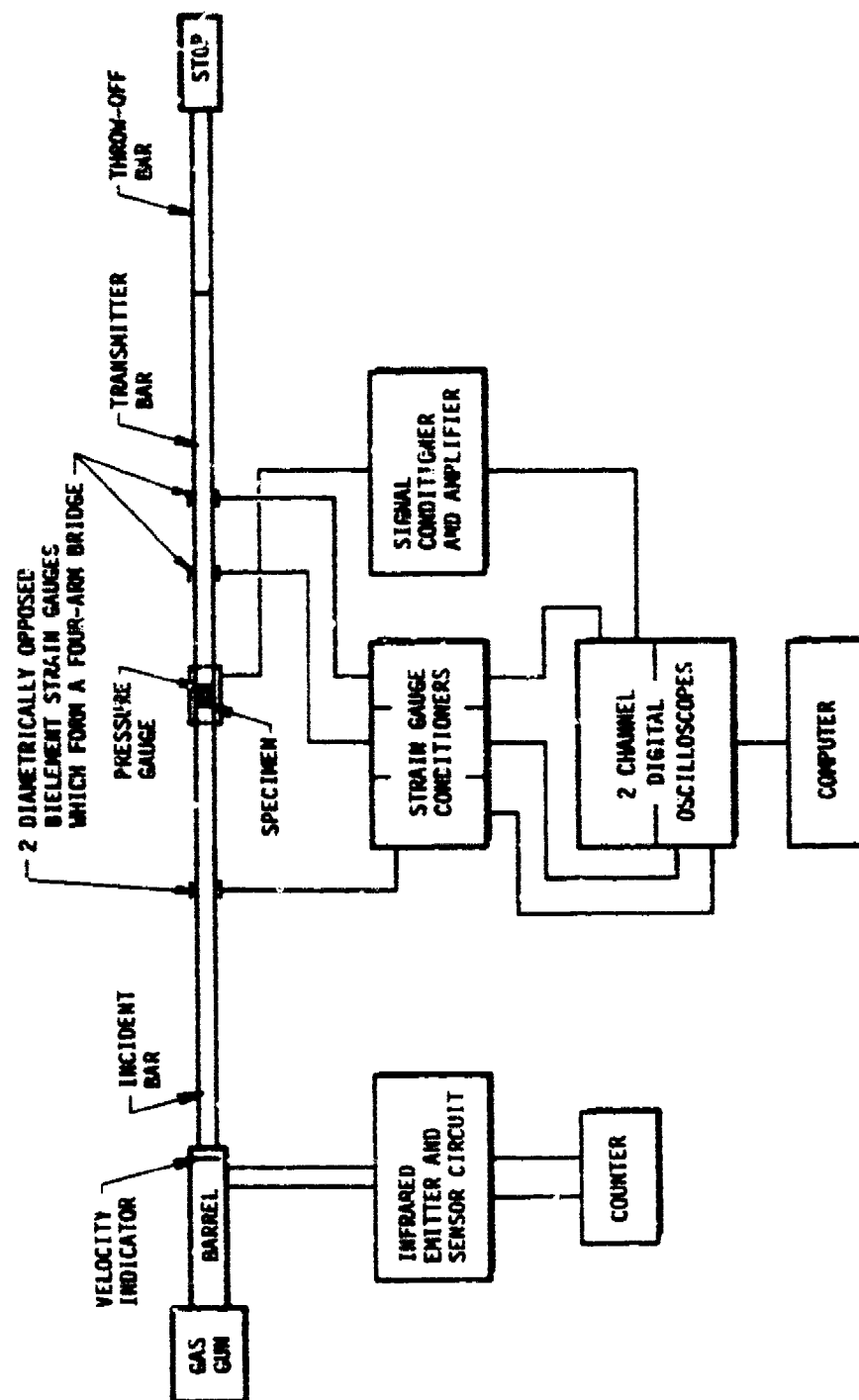
Figure 9. Schematic of Electronic Data Recording System.

19

TABLE 2. LIST OF ELECTRONIC EQUIPMENT

Item	Manufacturer	Specifications
Pressure Transducer	PCB Model 102A04	Max Pressure 10,000 psi
Signal Conditioner	PCB Model 483M37	Six Cnannels Fixed gains of 1, 10, or 20
Counter/Timer	HP Model 5315-A	Two Channels
Oscilloscope (Digital)	Nicholet Model 204-A	Two Channels
Strain Gauge	Micro Measurements EA-06-250TB-350-LE	Bielement
Strain Gauge Conditioner	Measurements Group Inc. Model 2311	Tnree Channels

SECTION III
EXPERIMENTS AND RESULTS

A.   SHPB Tests

   1. Small-Diameter SHPB Tests

   Initial SHPB tests were conducted in a 0.5 inch (1.27 cm) diameter
operational SwRI SHPB normally used for dynamic stress-strain data of metal
specimens.

   Several different materials were used as test specimens. These
materials are listed in Table 3, along with test parameters, while results of
these tests are given in Table 4.

   2. Large-Diameter SHPB Tests.

   a. Calibration

   As described earlier in Subsection I.B.2, a 2-inch (5.08 cm)
diameter SHPB was designed and installed in a laboratory at SwRI. Checks on
the expected velocity and incident pressure were made using three different
ways. First, based on Equations (1) and (2), a predicted velocity for the
desired incident stress was determined. A second check was obtained from a
time measured by the velocity-measuring device. The measured time, divided
into the distance between light sensors of the velocity device, gave the
velocity of the striker bar. Using this velocity, an approximate incident
pressure was calculated, using Equation (2). The third check came from the
output of a strain gauge mounted on the incident bar. Using the known voltage
output of the strain gauge, the given gauge factor, and the modulus of the bar
material, the stress level was calculated. The SHPB was operated initially at
several chamber pressures and the velocity gauge output agreed within 1
percent of the predicted velocity from Equation (1). The output of the
incident bar strain gauge, shown typically in Figure 10, was estimated to
agree within 2 percent of the stress calculated, using a combination of
Equations (1) and (2).

21

TABLE 3. DATA FOR SMALL-DIAMETER SHPB TESTS

Test No.	Mat'l	Specimen Length (in)	Specific Weight (lb/ft³)	Projectile Length (in)	Projectile Velocity (in/s)
3*	Sand	1.928	112.7	4.0	1057
4	Sand	2.225	101.2	4.0	1092
5	Sand	2.065	103.4	4.0	1080
6	Sand	2.225	102.0	4.0	912
7	Sand	2.025	104.4	4.0	1057
8	Glass**	2.098	84.2	4.0	395
9	Clay	2.922	84.8	4.0	1073
10	Clay	1.479	104.6	4.0	399
11	Glass	2.160	89.8	4.0	1087
12	Glass	2.123	88.6	4.0	1080
13	Glass	2.250	88.0	4.0	1075
14	Glass	2.255	85.2	4.0	1057
15	Glass	2.315	91.4	4.0	1055
16	Glass	2.185	89.7	4.0	1068
17	Glass	2.111	95.6	4.0	1073
18	Glass	2.161	89.8	4.0	1080
19	Glass	2.264	90.0	4.0	1059
20	Clay	2.195	91.9	4.0	–
21	Clay	2.213	98.2	4.0	1055
22	Clay	2.014	81.9	4.0	1066
23	Clay	2.296	96.3	4.0	1075
24	Clay	2.215	90.2	4.0	1073

*   Test numbers 1 and 2 not recorded.
**   3 mm diameter glass beads.

22

TABLE 4. RESULTS OF SMALL-DIAMETER SHPB TESTS

Test No.	Incident Stress, σ_I (psi)	Transmitted Stress, σ_T (psi)	σ_T / σ_I	Specimen Wave Speed c, in./sec.
3	78090	1970	0.025	13830
4	78090	1180	0.015	19500
5	78090	1054	0.014	20170
6	36480	790	0.012	19500
7	77040	1380	0.018	22360
8	29130	345	0.012	24219
9	78090	750	0.010	30920
10	29130	1100	0.038	20970
11	78090	1540	0.020	29090
12	78090	1190	0.015	30060
13	77040	1850	0.024	33780
14	77040	1840	0.024	25650
15	77000	541	0.007	32340
16	77670	1830	0.024	33185
17	79360	1015	0.013	28250
18	79020	1559	0.010	40090
19	77670	605	0.005	34370
20	77670	853	0.011	33620
21	77670	1274	0.016	35300
22	77670	268	0.003	29600
23	79700	917	0.012	33290
24	79020	414	0.005	33580
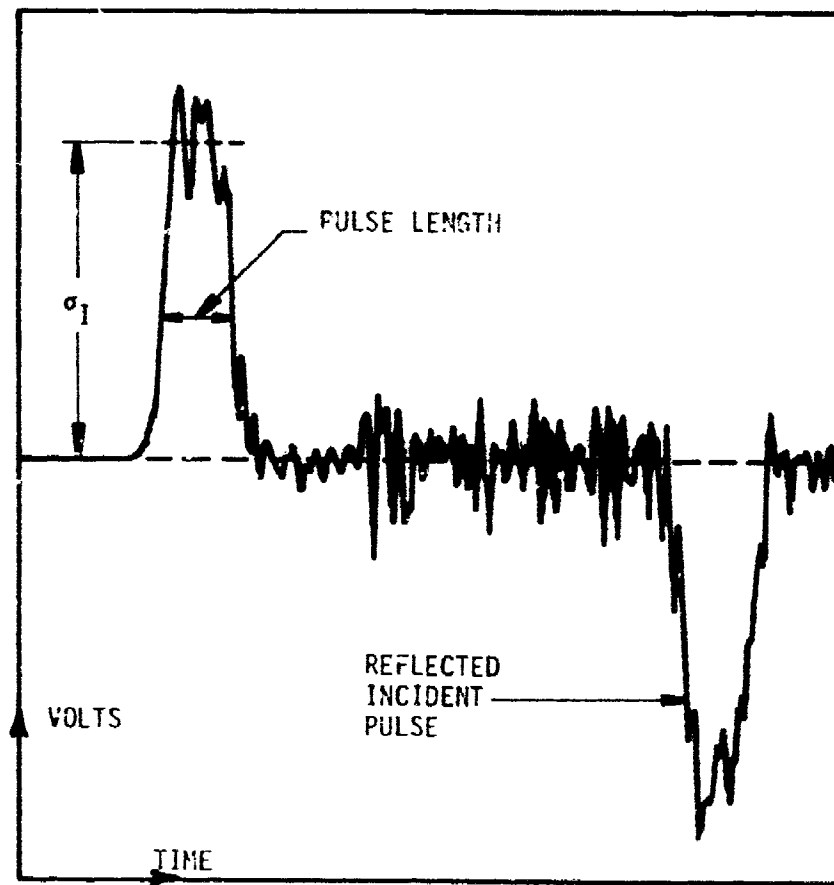
Gas Gun Chamber Pressure = 84 psi. Striker
Bar Velocity = 1026 in/sec. Incident stress
σ_I = 75110 psi. Striker Bar length = 3.0 in.

Figure 10. Typical Output of SwRI Split-Hopkinson Pressure
Bar Strain Gauges.

PRESSURE AND TRANSMITTED PULSES AS A RESULT OF THE SECOND INCIDENT PULSE

TRANSMITTED PRESSURE NO 1 540 PSI

PRESSURE GAUGE 396 PSI

200 usec

50/80 DRY SAND, 4 IN LONG SPECIMEN
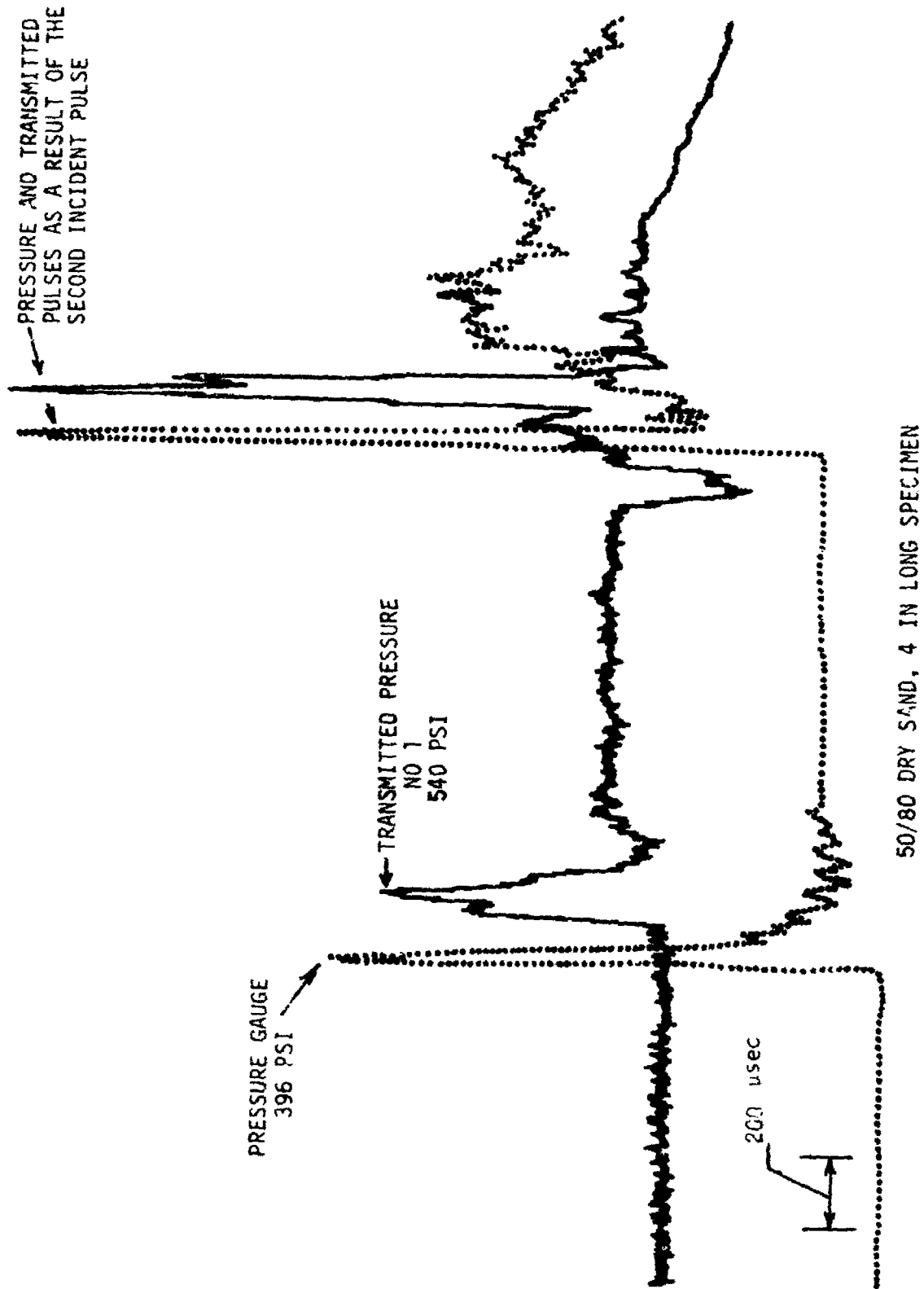
FIGURE 10. Typical output of SwRI Split-Hopkinson Pressure Bar Strain Gauges (continued).

SECOND INCIDENT
PULSE

TRANSMITTED
PRESSURE NO 2
600 PSI

INCIDENT PRESSURE
35000 PSI

REFLECTED
PRESSURE

100 μsec
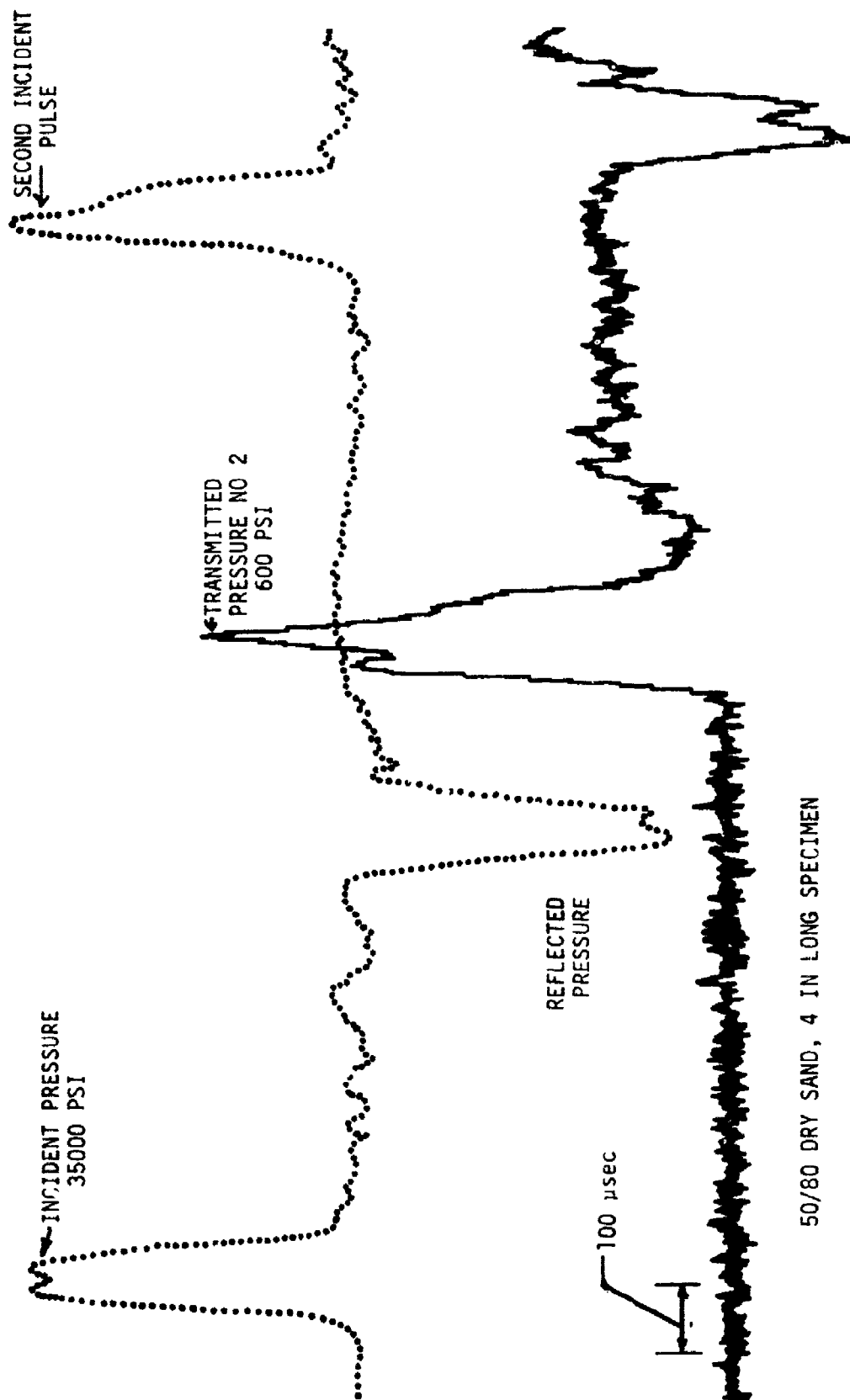
50/80 DRY SAND, 4 IN LONG SPECIMEN

FIGURE 10. Typical output of SwRI Split-Hopkinson
Bar Strain Gauges (concluded).

26

The pulse of Figure 10 was chosen to show the degree of noise experienced in output at some impact velocities. The noise is mechanical and is only masked by electronic filtering. It was found that much of the noise could be eliminated by applying a small amount of silicon grease between the striker bar and the incident bar.

The oscillations that appear near the peak of the incident pulse in Figure 10 are often referred to as Pochhammer-Chree oscillations and are a result of wave dispersion. A Pochhammer-Chree solution of the cylindrical wave equation (References 10-11) accounts for lateral inertia which include higher-frequency components, and these higher-frequency components travel at a lower wave speed than the lower-frequency components. The higher frequency components then lag behind the main body of the pulse, causing ripples or oscillations in the main body of the pulse as well as some oscillations following the main pulse. A good discussion of this and corrections are found in Reference 12.

b. Noise to Signal Problems

As shown in Figure 10, considerable noise is evident in the output of the strain gauges. This noise causes a definite problem when one tries to determine the portion of the pulse transmitted into the soil specimen from the incident bar.

Assuming the general shape of elastic pulses are unchanged during the reflection/refraction process, then a relation between impulse of the incident reflected, and refracted (transmitted) pulse may be written as

$$I_I + I_R = I_T, \qquad\qquad (3)$$

where I represents impulse and the subscripts I, R, and T represent incident, reflected, and transmitted, respectively. Since the pressure level for the reflected pulse is opposite in sign of the incident pulse, then the left-hand side of Equation (3) represents the difference of I_I and I_R. For the steel/soil interface a reasonable value of I_T is approximately 2 percent of

I_I. This means that the time integral of the incident pulse less the time integral of the reflected pulse of Figure 10 is approximately 0.02 l_I. Considering the noise and oscillations in each pulse plus the uncertainty of where each pulse starts in time, then the expected 2 percent could be in doubt by orders of magnitude. In an effort to determine the pressure level in the soil specimen just downstream of the incident-bar/soil interface, software was written to calculate the impulse and average pressure for the incident and reflected pulses. When applied to many of the recorded pulses, so many variations and physically improper data were obtained, that the results were not included in the final report. The inability to gain these data leads to the necessity for testing at higher-stress levels or using a lower-characteristic impedance bar material.

c. Dry Soils Tests

The procedure for testing dry soils was also used in the test of moist soil specimens such that a uniform specimen preparation procedure was established and used for all soil specimens.

In the specimen preparation, the pressure gauge holder was placed on a table top with pressure gauge end up (See Figure 11). A spacer designed to keep the pressure gauge leads outside the steel sleeve was placed around the pressure gauge holder. If the pressure gauge was to be used in the experiment, the face of the gauge and the cap (Figure 6) were left uncovered and the soil was placed on top of the cap face. If the wafer was to be used in the experiment, the pressure gauge was removed from the cap and the wafer was placed on top of the cap before the soil was placed in the sleeve. After placement of the pressure gauge or wafer, a portion of the soil was placed in the sleeve. If the specimen was built up in two layers, then half the soil at a time was placed in the sleeve, and, if specimen was built up in four layers, then a quarter of the soil was used for each layer. The compacting rod was used and compaction to a designed height was done on each layer. Compaction was accomplished using a solid cylinder weighing approximately 3 pounds.

In all soil tests, whether dry or moist, a dry specific weight of 100.0 lbs/ft^3 (1.6 g/cc) was used. For a 4-inch (10.16 cm) long specimen, a

THIS END TAPPED WITH
3.0 LB HAMMER

STEEL SLEEVE

SHIM OR WAFER
WITH 'O' RING

SOIL
SPECIMEN

WAFER WITH 'O' RING OR
PRESSURE GAUGE FACE

PRESSURE GAUGE

PRESSURE
GAUGE
LEAD

SPACER

PRESSURE GAUGE HOLDER

TABLE TOP
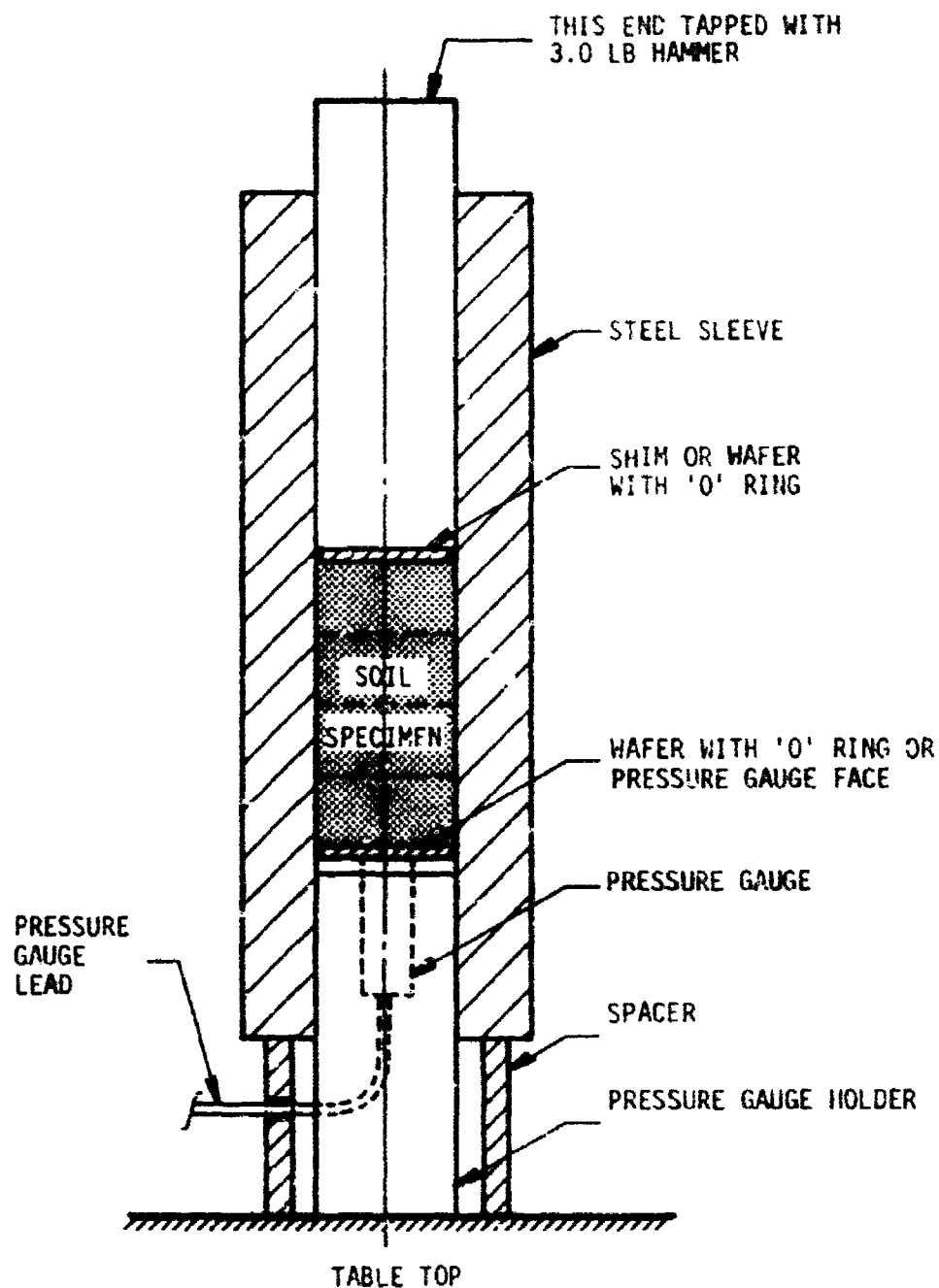
Figure 11. Soil Specimen Assembly.

29

dry soil weight of 0.73 pounds (330 grams) was compacted to the proper length. This means that, for the moist specimens, the density increased as moisture content increased.

After all the soil was compacted to the proper height, the steel shim, or wafer, was placed on top of the specimen and tamped in place to assure proper location. This placement could be a source of error if all the air is not removed from the top of the specimen.

If the pressure gauge was in use, the pressure gauge holder was held in place while the specimen holder was placed in the SHPB position. If the pressure gauge was not in use, the wafer was held in place by friction of the "O" ring against the steel sleeve.

After the specimen holder containing the specimen and pressure gauge holder was placed in the SHPB, bars were pushed by hand into the front end of the specimen holder and against the back end of the specimen holder as shown in Figures 6 and 7. Alignment was adjusted as best as could be by eye, and a plastic aligning collar was placed at the interface of the pressure gauge holder and the transmitter bar. When an axial load for confining pressure was used, a hydraulic jack was placed in series with and at the end of the throw-off bar. For the axial load tests the incident bar was held fixed by a rubber collar and hose clamps at the journal bearing just downstream of the striker-bar/incident-bar interface.

Striker bar lengths of 4 inches (10.16 cm) and 8 inches (20.32 cm) were used in the preliminary tests, and a decision was made to use the 8 inches (20.32 cm) length for all tests. Varying the specimen length then gives a change in the ratio of striker bar length to specimen length. Specimen lengths of 2 inches (5.08), 4 inches (10.16), and 6 inches (15.24) inch (cm) were used for tests of both dry sand, and only 4 inches (10.16 cm) long specimen were used in tests for moist sand. In addition, some tests of 0.5 inches (1.27 cm) and 1 inch (2.54 cm) length dry sand specimens were conducted.

Two different dry sand particle sizes were tested using the thin shim in front of the specimen and the pressure gauge holder to the rear of the specimen (See Figure 6). Both sand specimens were of fused silica with 50/80 and 20/40 size designation. The 50/80 sand is a medium to fine sand with 50 percent of the grain size between 0.2 and 0.3 mm. The 20/40 sand is a coarse to medium sand with 50 percent of the grain size between 0.4 and 0.8 mm. The ratios of transmitted peak stress to incident stress are shown in Figure 12. Ratios of peak pressure to incident stress for these tests are shown in Figure 13. For these tests only two-layer compaction was used in specimen preparation.

In addition to the two sizes of sand particles, a silica flour, designated 240, was tested. The material designation means that the particle size is smaller than 0.06 mm and it is essentially a powder. Because this material was very difficult to confine, limited tests were conducted. Results of the test on the silica flour are also shown in Figures 12 and 13.

For the 50/80 dry sand wave speed was determined experimentally and is shown along with the transmitted stress ratio in Figure 14. In addition, the 50/80 dry sand was tested with a confining axial load applied in series of the bar. Stress levels of the static axial compression were measured using the strain gauges on the transmitter bar. Axial static compressive stress up to approximately 300 psi (2.4 MPa) were used and results of those tests are shown in Figure 15.

d. Moist Soil Tests

Dry soil of the same 50/80 stock was mixed with tap water to produce specimens of varying moisture content. The void content and moisture content are related by

31
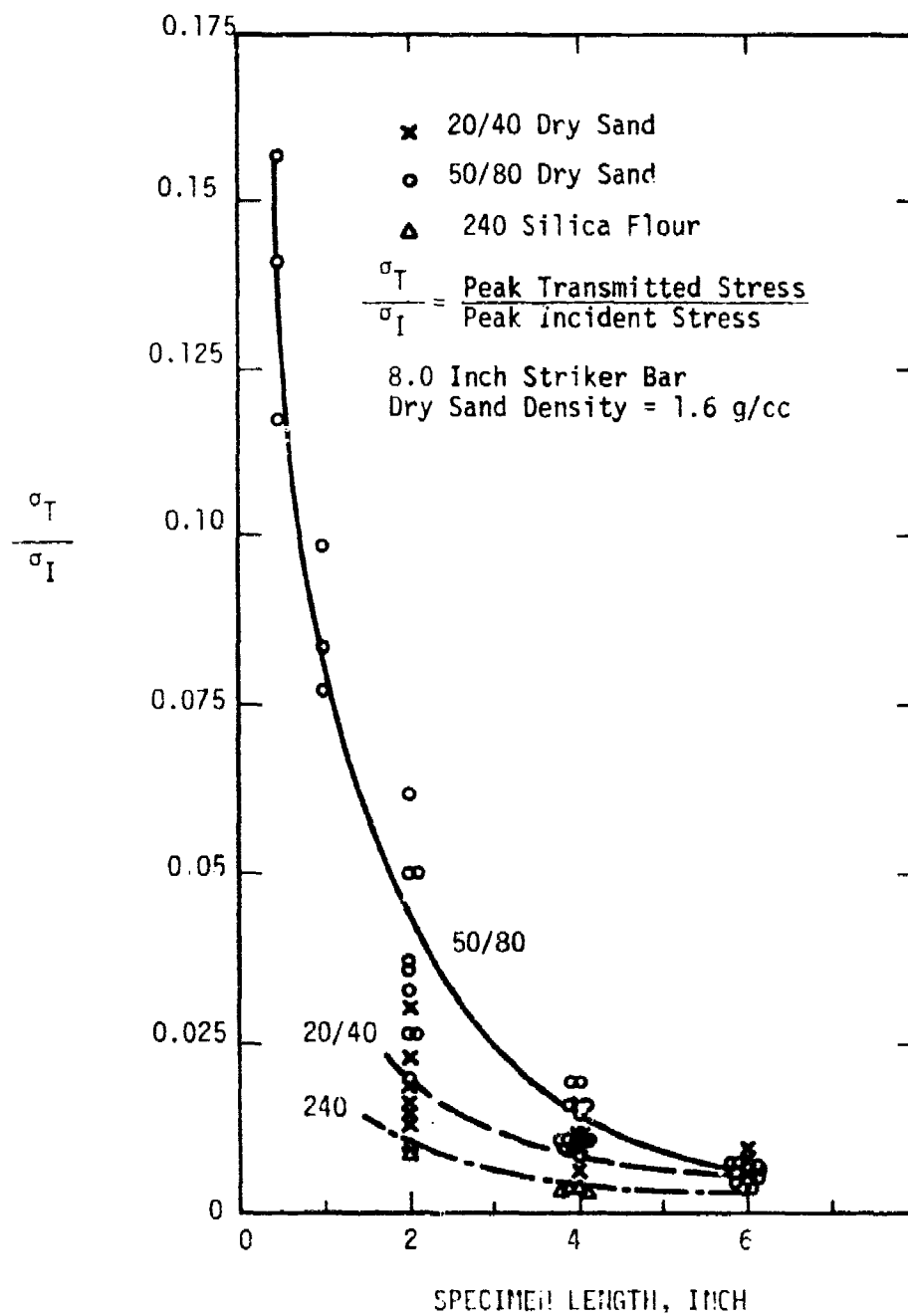
Figure 12. Transmitted Stress Ratio Vs Specimen Length for Dry Sand.

32
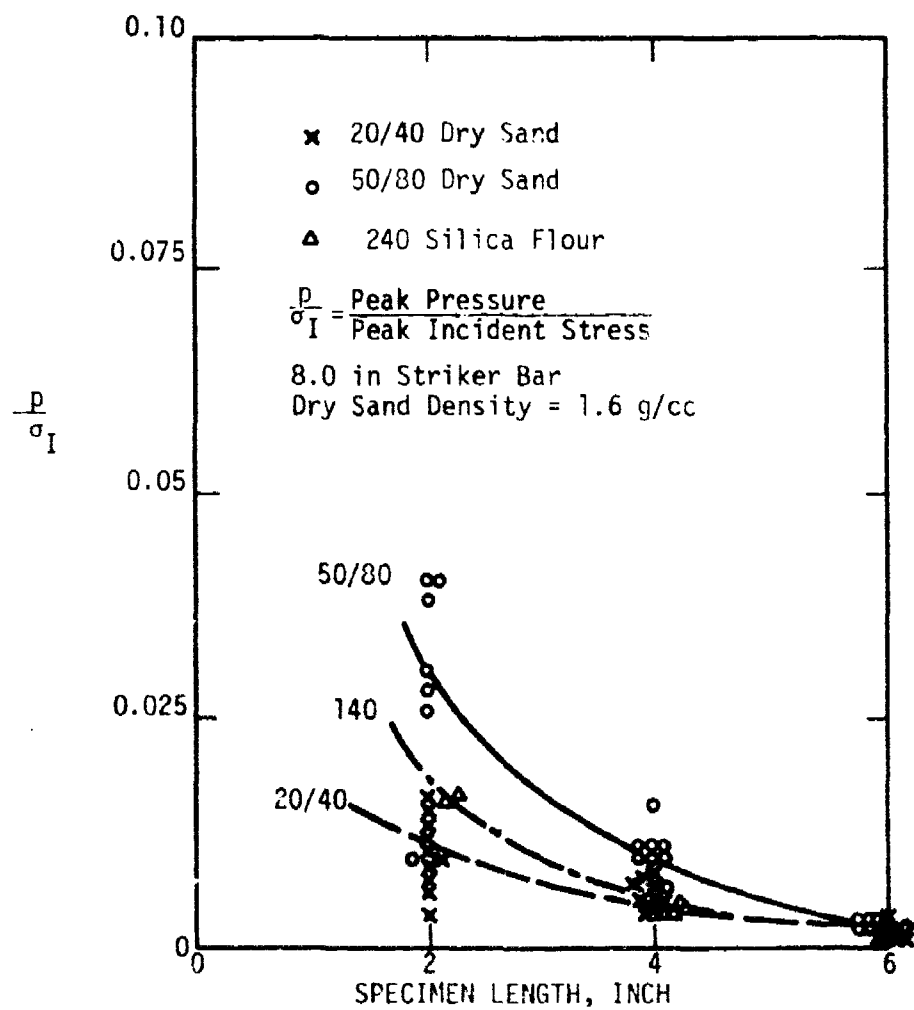
Figure 13. Pressure Ratio Versus Specimen Length for Dry Sand.

33
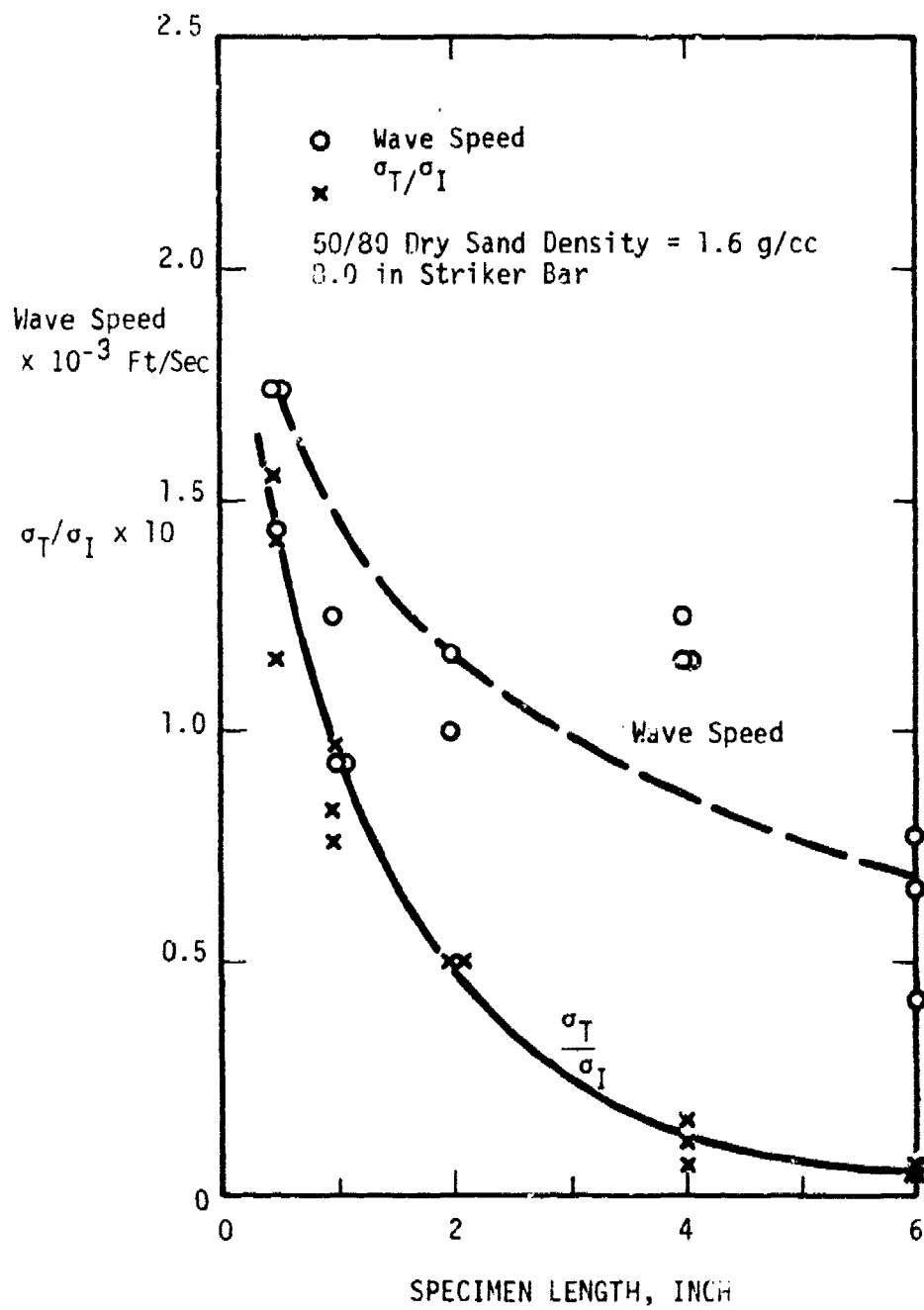
Figure 14. Transmitted Stress Ratio and Wave Speed Versus Specimen Length.

34
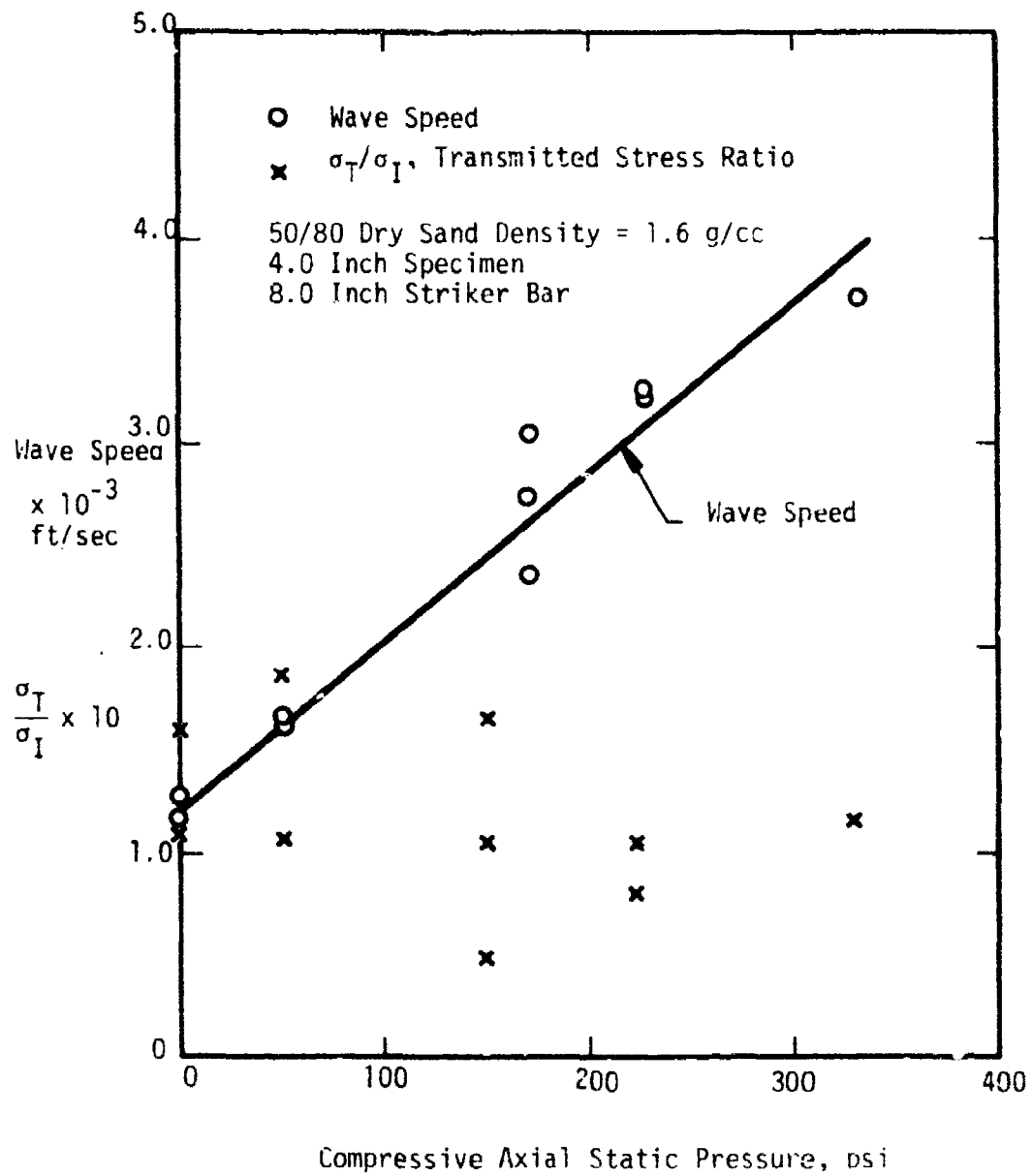
Figure 15   Effect of Static Axial Compression on Wave Speed and
Transmitted Stress Ratio.

$$\frac{S}{S_m} = \frac{(1 + w)}{(1 + e)} \tag{4}$$

where
- S = specimen density
- S_m = solid material density = 2.65 g/cc
- w = moisture content
- e = void content

For all tests the dry density was maintained constant at 1.6 g/cc. Using this density, Equation (4), and $w = 0.0$, the void content for the dry 50/80 sand is calculated to be 0.66. For complete saturation the moisture content is given by

$$w = e/S_m \tag{5}$$

and for $e = 0.66$ and $S_m = 2.65$ g/cc the saturation moisture content is 0.25.

Tests were performed at varying moisture contents in a specimen configuration using the shim as shown in Figure 6. The shim was not satisfactory for containing moisture and additional tests were conducted using steel wafers in the specimen configuration of Figure 7. As indicated before the dry density of the specimen was maintained constant; therefore, for a moist specimen, a known amount of soil plus water was forced into the dry density volumes. For these tests the density and specific volume of water was assumed to be unity. As might be expected, compaction of the moist specimens required more energy than the dry specimens except for those specimen at or near complete saturation. For the completely saturated specimen just the slightest compaction caused the soil particles to settle to the bottom and water to appear at the top of the specimen.

The results of the moist specimen tests using the specimen configuration of Figures 6 and 7 and a two-layer compaction are shown in Figure 16. Moisture content was determined from small amounts of soil specimen material taken at the beginning of each test. Each sample was dried overnight.

36
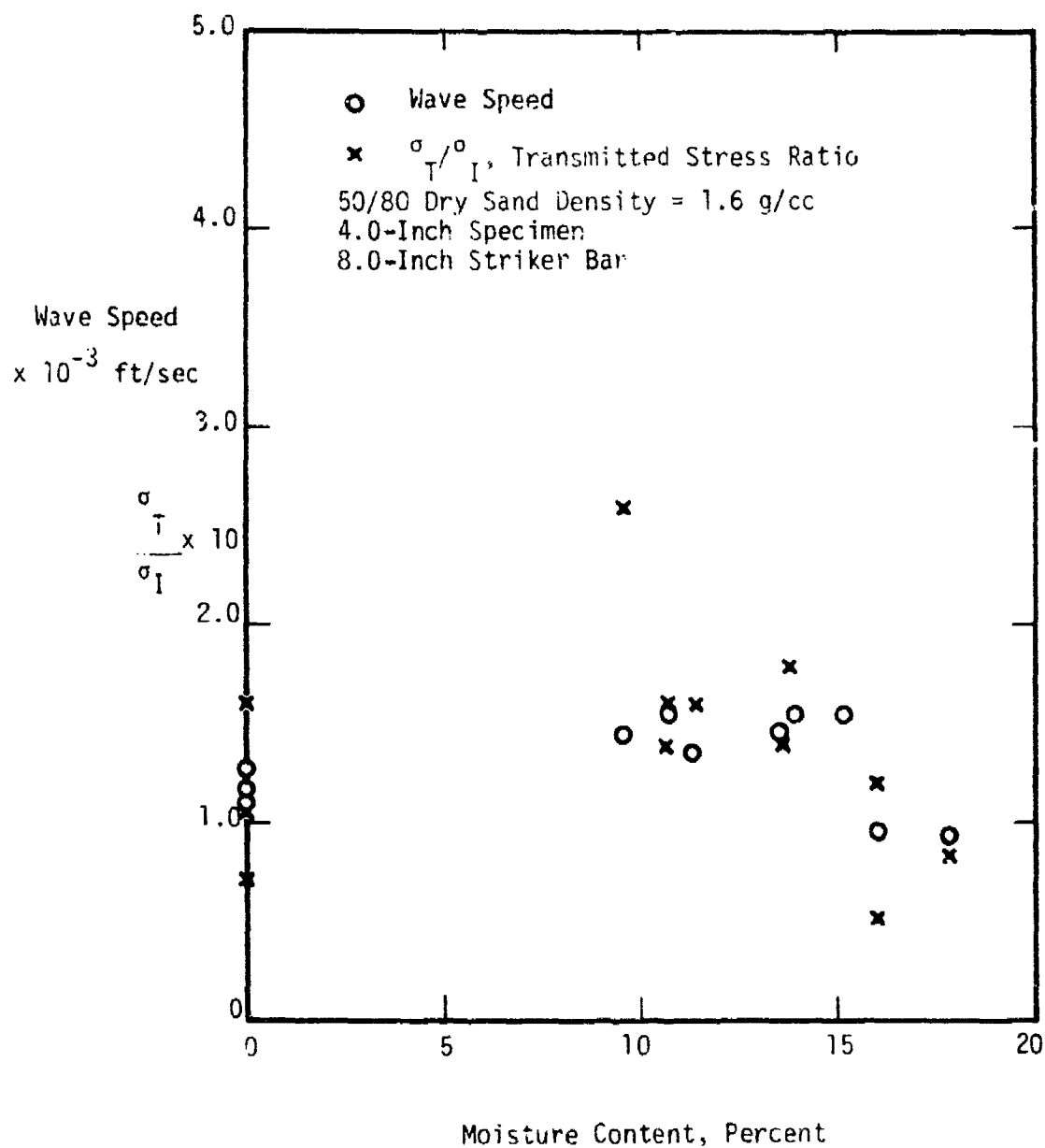
Figure 16. Effect of Moisture Content on Wave Speed and Transmitted Stress Ratio.

37

e. Glass Bead and Steel Ball Tests

BB size steel balls and 3.0 mm glass beads were also tested in the same manner as described above. In each case the beads or balls were poured into the specimen holder to a proper length and a shim was placed at the top. Only a few tests of each were performed and results will be discussed in Section IV.

B. STATIC SOIL STRESS-STRAIN CURVES

1. Introduction

During the moist specimen tests a question arose as to what effect the moisture content has on wave speed and transmissibility near the region of complete saturation. Both transmissibility and wave speed were expected to increase with increase in moisture content, most especially near saturation. The wave speed in water is approximately 5000 ft/sec (1524 m/sec) and for the dry soil specimens it is approximately 1200 ft/sec (366 m/sec). Comparing these two values, where does the increase in dry-to-moist specimen wave speed begin, or is it a rather abrupt jump very near saturation? There is no indication from Figure 16 that an increase in wave speed is occurring and the question arose as to whether compaction during specimen preparation could affect the transmitted stress ratio of both dry and moist specimens. With these thoughts in mind, a series of static stress-strain curves at different compactions was obtained. The specimen holder used in the SHPB tests was also used in the static tests.

2. Effects of Compaction

A set of three stress-strain curves for two-layer compaction specimens of 50/80 dry sand were obtained from a screw machine material tester. These curves were not reproducible at all and were widely scattered. A set of three stress-strain curves was obtained for four-layer compaction specimens of 50/80 dry sand. These three curves showed very good reproducibility, and, as a consequence, all other tests were done, using four-

38

layer compaction. The static stress-strain curves were carried up to 1500 psi (10.3 MPa) and approximately 4 percent engineering strain.

3. Soil Tests

Tests on dry and moist 50/80 sand were carried out in a material tester using the same steel sleeve and specimen preparation used in the SHPB tests. All tests were conducted using a four-layer compaction procedure and tested without a steel wafer between the 2.0 inch (5.08 cm) diameter loading bar and the soil. An initial test was performed to determine the force or stress required to move the wafer with "O" rings. Based on the specimen cross section area this stress is approximately 8.0 psi (55.2 KPa). Results of dry and moist sand static tests are shown in Figure 17.

A sieve analysis of the 50/80 sand was accomplished and the results are shown in Figure 18. The density of the solid sand particles was experimentally determined to be 2.65 g/cc.
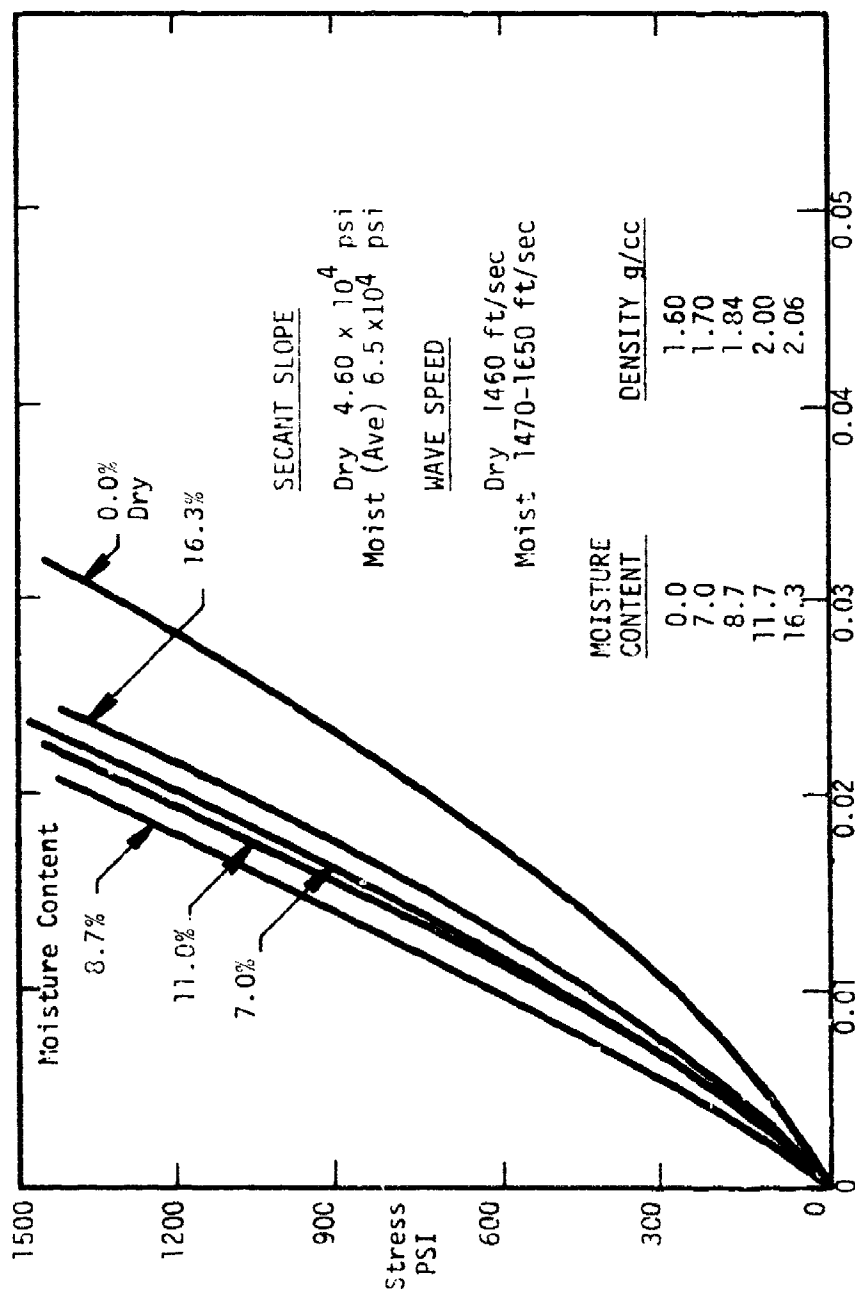
Figure 17. Static Stress Strain Curves for 50/80 Sand Using Four Layer Compaction.

40
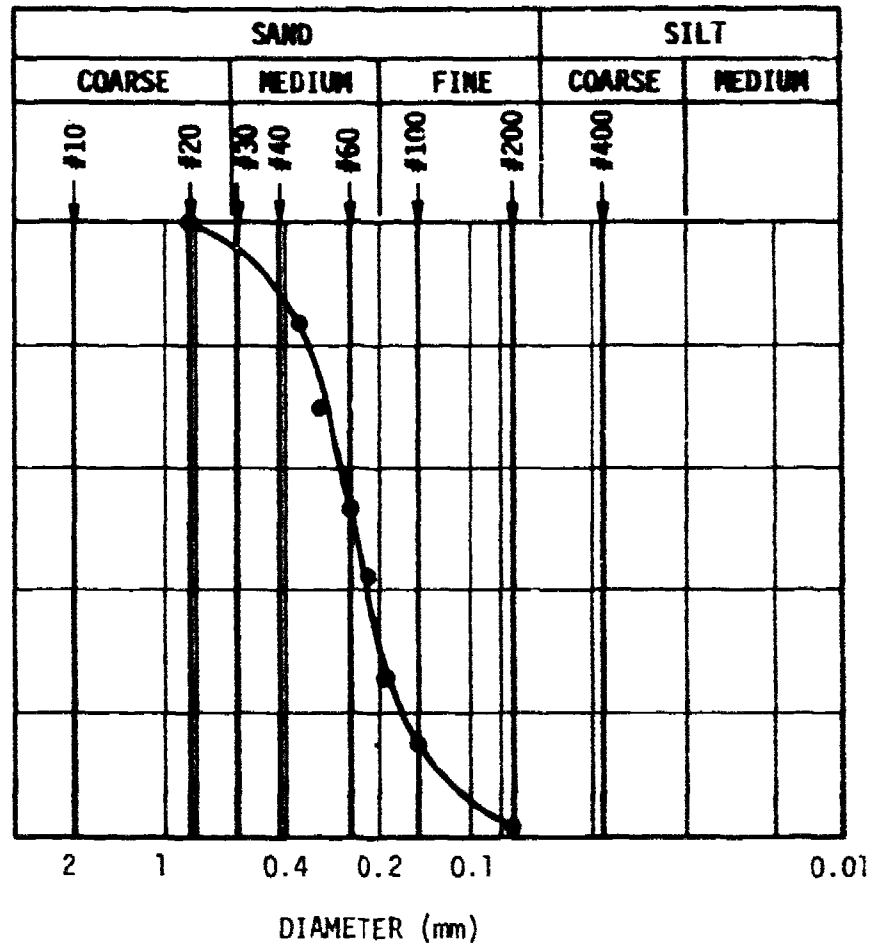
Figure 18.   Sieve Analysis of 50/80 Silica Sand.

41

SECTION IV
DISCUSSION OF SOIL TEST RESULTS

A.   SHPB Tests

1. Attenuation From Material Damping

If one treats the interaction of the steel and soil as an elastic response, then equations given in Appendix A apply. The peak stress level in the soil σ'_I just downstream of the incident-bar/soil interface for an elastic system is related to the peak incident stress σ_I by the expression

$$\sigma'_I = \sigma_I \left[\frac{2(\rho c)_S}{(\rho c)_B + (\rho c)_S} \right] = K_{BS} \, \sigma_I \qquad (4)$$

where K_{BS} is the transmission coefficient from bar B to soil S, (ρc) is the characteristic impedance, and the subscripts S and B denote soil and bar, respectively. The defined stresses σ_I, σ'_I, σ''_I and σ_T are shown in Figure 19. Assuming an exponential decay for material damping (Reference 7, p. 246), the stress σ''_I may be written in terms of the stress σ'_I as

$$\sigma''_I = \sigma'_I \, \exp\,(-\alpha\Delta L) \qquad (5)$$

where α is a damping coefficient, ΔL is the distance between the positions of the two stresses, and geometrical damping is neglected. Using the same general relation similar to Equation (4), the theoretical elastic relation between σ''_I and σ_T may be written as
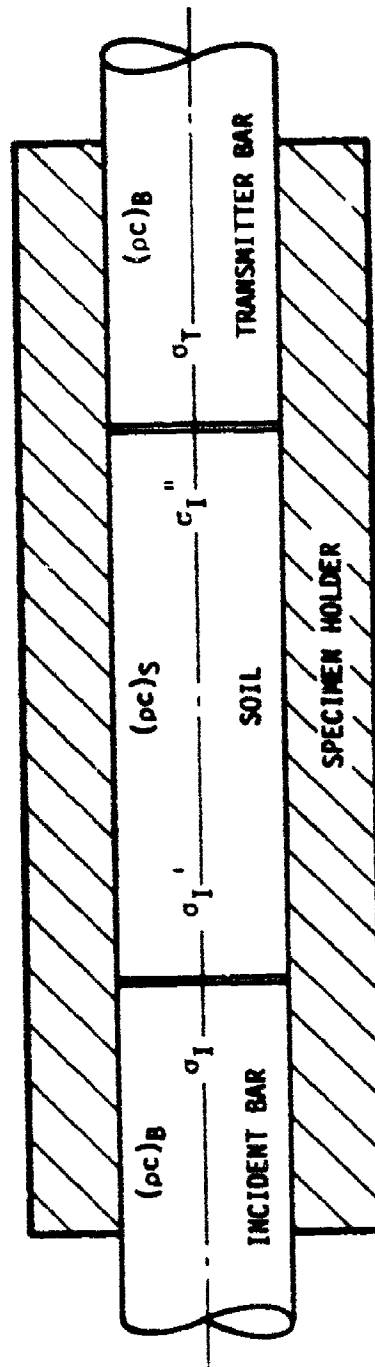
Figure 19. Schematic of Soil Specimen Showing Various Stresses.

43

$$\sigma_T = \sigma_I'' \left[\frac{2(\rho c)_B}{(\rho c)_B + (\rho c)_S} \right] = K_{SB} \sigma_I'' \tag{6}$$

where σ_T is the stress in the transmitter bar and K_{SB} is the transmission coefficient from soil S to bar B. Combining the Equations (4), (5), and (6), the relationship between the peak incident stress σ_I and the transmitted stress σ_T may be written as

$$\frac{\sigma_T}{\sigma_I} = K_{SB} \, K_{BS} \, \exp(-\alpha \Delta L) \tag{7}$$

Based on experimental values of wave speeds shown in Figure 14, the average wave speed is approximately 1200 ft/sec (365.9 m/sec) for a specific weight of 100 lb/ft^3 (density of 1.6 g/cc). Using these values and the corresponding values of 16,700 ft/sec (5080 m/sec) and 490 lb/ft^3 (7.84 g/cc) for the steel bar, the product $K_{SB}K_{BS}$ is 0.043. Using this product as a constant, the expression for the damping coefficient becomes

$$\alpha = \frac{-1.0}{\Delta L} \ln \left(17.5 \, \frac{\sigma_T}{\sigma_I} \right) \tag{8}$$

where ΔL is the length of the specimen in feet associated with the ratio σ_T/σ_I. A range of values for each specimen length is shown in Table 5, along with values taken from references as indicated.

The negative number shown for the 2-inch specimen of the SHPB test indicates that the downstream stress is higher than the upstream stress at the incident-bar/soil interface. Two things may explain this, i.e., the wave speed in the specimen increases with increasing stress and decreasing specimen length and the short specimen length is beginning to act as a normal SHPB specimen where wave reflections within the specimen become important. For a 25 percent increase in wave speed of the 2-inch length specimen in the SHPB of

44

TABLE 5.   DAMPING COEFFICIENTS FOR DRY SAND

α, Damping Coefficient, 1/FT

ΔL (in)	SHPB 50/80 SAND	Reference 13 OTTAWA SAND	Reference 14 OTTAWA SAND
2	(-.31) - 4.95	0.57-1.73	*
4	3.14-6.29	0.60-1.53	*
6	4.06-5.89	0.63-1.39	*
10	*	0.51-1.26	2.78-3.47

* NO DATA

Table 5, the α range becomes 1.0-6.2. Damping coefficients of Reference 14 are given in terms of the logarithmic decrement δ.   The damping coefficient may be expressed in terms of the logarithmic decrement by the expression

$$\alpha = \frac{f\delta}{v} = \frac{\delta}{vT} \qquad (9)$$

where f is pulse frequency, T is period of the pulse, and v is wave speed. For α in units of 1/ft then v must be in ft/sec and T in seconds. In Equation (9) the ratio f/v is actually the pulse length in feet. In comparing the data from SPHB and Reference 14, the data of Reference 14 were extended over a range of several orders of magnitude and may not be applicable. The data of Reference 14 were obtained by a resonant column experiment at confining pressures up to 50 psi (.34MPa).

The data in Reference 13 were taken in a 5.0 foot (1.52 m) long, 28 in (7.1 cm) diameter horizontal tube filled with Ottawa sand. The loading was applied by an air shock through a thin membrane. Peak pressures up to 300 psi (2.07 MPa) were recorded by soil stress gauges. Stress attenuation was displayed by a curve of normalized stress versus distance along the tube of soil.

45

2. Effects of Moisture Content

Results of Reference 14 show a definite increase in damping at
saturation. The effects of moisture content for the SHPB test shown in Figure
20 show a decrease in damping with increasing moisture content, but, at or
near saturation, a definite increase in damping is evidenced by the decrease
in transmitted stress ratio. A slight increase in wave speed with moisture
content is evident up to about 50 percent saturation (12-15 percent moisture)
and then a decrease in wave speed down below that of dry sand is evident at
saturation (25 percent). This observation agrees with compressive wave speed
results of both saturated Ottawa and quartz sand, tested in Reference 15. The
same trends are also observed for Edgar Plastic Kaolin (EPK) clay of Reference
13.

The effects of moisture content on wave speed in the SHPB tests,
transmitted stress ratio in SHPB, and on the stiffness or slope of stress-
strain curve in the static tests are assumed to be of the same origin. Small
amounts of air or gas at or near saturation would seem to have the same effect
on all these three items. For a given soil void content, a small amount of
water stiffens the soil and increases the slope of the static stress-strain
curve, increases the transmitted stress ratio, and tends to increase wave
speed; however, the wave speed is offset by the increased density of the
specimen. In the moist specimens of the SHPB tests, a constant dry density
was maintained by proper compaction. With increasing moisture content for a
given dry density and void ratio, stiffness caused by compaction of the
specimen increased up to an optimum moisture content, after which this
stiffness decreased with increasing moisture content. This phenomenon is
discussed in detail in texts on soil mechanics such as Reference 16.

With increasing moisture content up near saturation, the amount of
the void space filled with air or gas i.e., gas content has a very strong
influence on stiffness and wave speed. For instance, the effect of small
amounts of gas on wave speed at saturation is such that the wave speed may be
almost halved for 1 percent gas content. Gas content here means a fraction of
pore space of the dry specimen. For a porosity of 50 percent, a gas content
would mean 0.5 percent gas in the total specimen volume. This 1 percent gas
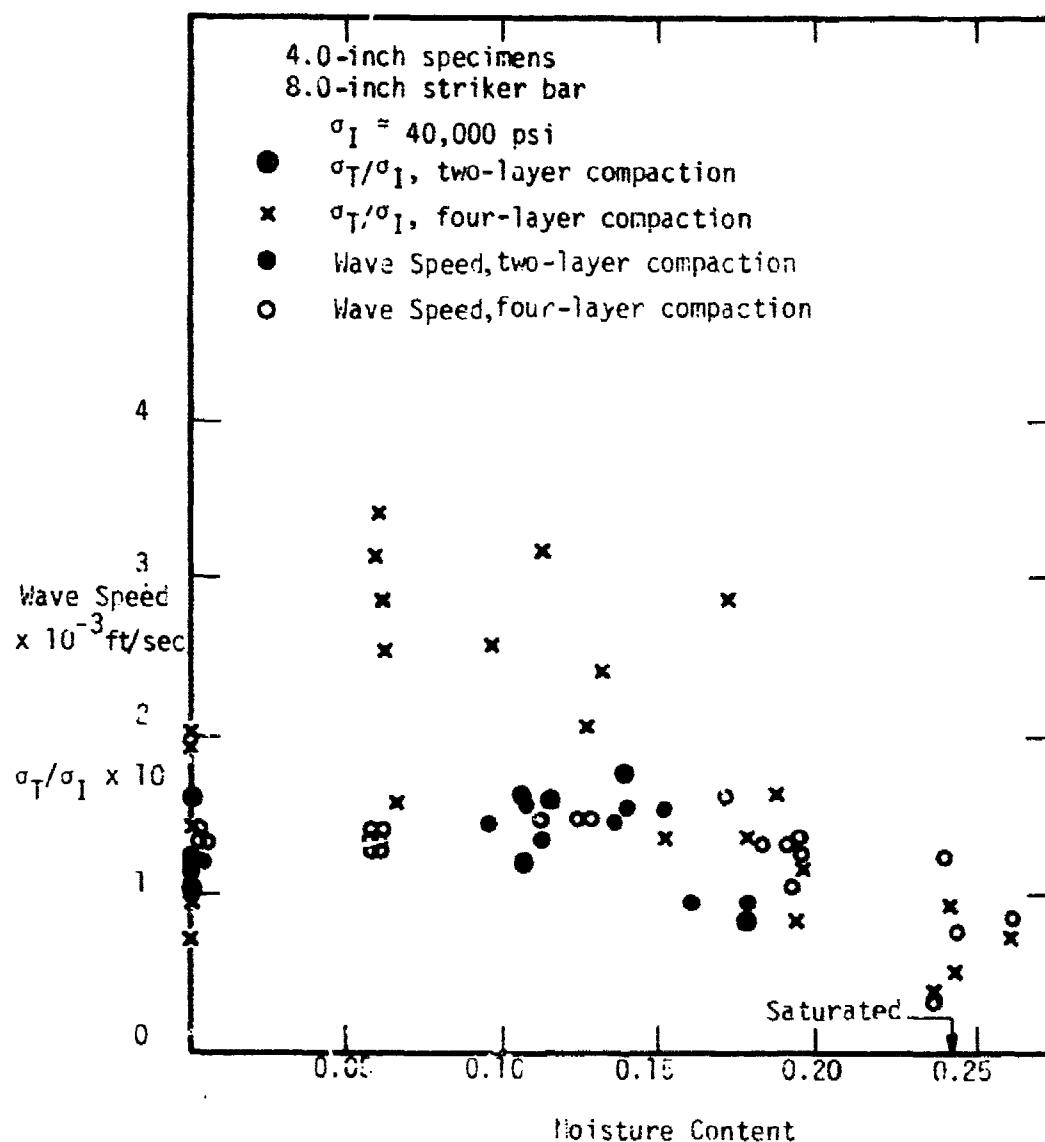
Figure 20. Effects of Moisture Content on Wave Speed and Transmitted Stress Ratio.

47

content would reduce the bulk modulus of the "almost saturated" soil specimen by approximately four. An excellent discussion of effects of gas content in soils is given in Reference 17.

The effect of the gas content in the soil-water mixture is probably the reason that a large increase in wave speed up to that of water-soil mixture near saturation is not found in the SHPB tests. During the SHPB test, no effort was made to reduce the gas content trapped in the pores of the mixture. However, it is important to point out that a small gas content will be found in regular soil. Nature does not necessarily have a vacuum pump to reduce this residual of gas in the pores of soil. However, one must temper such sweeping statements with the fact that considerable friction was present at the walls of the specimen holder in the SHPB tests, and this may influence all the data given in this report. As mentioned before, no procedures were followed to reduce or eliminate the wall friction in the SHPB tests.

3. Water Specimen

As a check on the SHPB system, the specimen holder was filled with tap water and an incident stress was applied to a 100 percent water specimen. The transmitted stress and wave speed were determined experimentally. Using the measured wave speed of 4780 ft/sec (1457 m/sec) and water density of 1.0 g/cc, the transmission ratio σ_T/σ_I = 0.136 was calculated using Equation (7), assuming α = 0.0. The experimentally determined value of σ_T/σ_I was 0.144. The reported value of wave speed is given in Reference 7 as 4800 ft/sec. This test was considered to be a rather rigorous test on the transmissibility capability of the SwRI SHPB system.

4. Soil Particle Size Effects

The effects of particle size are evident in Figures 12 and 13. In Figure 12 the transmitted ratio of the smaller grain size 50/80 sand varies from 1.25 to 2.25 times the transmitted ratio of the larger grain size 20/40 sand. This same comparison of pressure ratios for the two grain sizes of Figure 13 shows a slightly higher result even though the pressure ratios on

48

the average are only two-thirds that of the transmitted ratios. Remembering that the radius of the transmitter bar is approximately 16 times greater than the radius of the face of the pressure gauge, it is interesting that the differences in measured values with grain size, for the two devices, are not much larger. For both measuring devices the differences between measured values shows a decrease with decreasing specimen length. However, the differences between all measurements of the same kind are less at the longer specimen length. Also the measurements at the longer length specimens show less scatter than measurements of the shorter length specimens.

5. Pressure Measurements Versus Transmitted Stresses

The use of the pressure gauge at the end of the soil specimen, as shown in Figure 6, proved to be satisfactory. However, differences between measured values exist between the pressure gauge and transmitted bar strain gauges. The transmitted stress ratios, as shown in Figure 12, were always higher than the pressure ratios of Figure 13. These differences seem to the independent of the incident or applied stresses. When comparing pressure and transmitted stress, the larger differences occur for the smaller grain 50/80 sand. This means one gets a larger transmitted stress-to-pressure ratio for the smaller-grain sand than for the large-grain sand. This appears to be reverse of what is expected. One would think that as grain size goes down, the measured pressure and transmitted stress would approach each other. However, the ratio of pressure to transmitted stress does appear to remain constant with specimen length. The same type pressure tranducer used in the SHPB tests was also used in Reference 1, where measured pressures in soil were lower than those reported in other places in the literature.

6. Effect of Axial Compressive Preload

As discussed in a previous section, an axial preload was applied to the SHPB system by placing a hydraulic jack in series with the throw-off bar and the SHPB stop. Calibration of the transmitted bar gauges to measure the preload gave a direct reading of the applied pressure. The effect of the preload on the wave speed and the transmitted stress is shown in Figure 15. As evident in Figure 15, the wave speed shows a rather large increase with

increases in preload or confining pressure. However, very little increase in the transmitted stress with increase in preload is evident. These two observations agree with results of References 14 and 15. Results of Reference 14 show that dissipation in dry granular materials does not always decrease with increasing confining pressure but appears to be morr dependent on magnitude of applied stress or vibration magnitude. However, the results of Reference 15 show that, for dry granular materials, an increase in wave speed is almost always evident with increases in confining pressure. In Figure 15, the specimen length is constant at 4 inches which means the transmitted ratio does not reflect any changes in specimen length. If the preload tests were run for a 2 inch long specimen, then the magnitude of the transmitted ratio should be higher but still reasonably constant with preload pressure.

Static preload or compaction does not have the same effect on soil properties as dynamic compaction with changes in moisture content. It is not clear as to whether this phenomenon is evident in dry compaction or not. If so, this means that, in the dry specimen tests, the dynamic compaction brings the specimen up to some stiffness or dissipation level and any increase due to static compaction has little effect. However, extremely large confining pressures should have a definite influence on the transmission properties of the dry specimen.

7. Tests on Glass Beads and Steel Balls

Results of tests on 3.0 mm glass beads are given in Tables 3 and 4. These tests were conducted only in the small-diameter SHPB. The average transmission ratios closely approximate the values of the 20/40 sand although the glass beads are about five times larger in diameter than the 20/40 grains.

Steel BB size balls (0.177 inch diameter) were tested in the 2-inch diameter SHPB. Three tests were conducted with a preload of 100 psi on the SHPB. Transmission ratios of 0.034, 0.042, and 0.060 were obtained for an average of 0.045. This value is low by a factor of 5 if the measured wave speed and density are used in Equation (7) to calculate this value.

These tests were performed to determine a range of transmission ratio for various materials and no further comments shall be made on the applicability of the data.

B.   STATIC SOIL TESTS

Static tests at strain rates of approximately 2.0×10^{-4}/sec were conducted on 4 inch long dry and moist 50/80 sand specimens. Two-and four-layer compaction tests were conducted and it was found that the four-layer compaction showed less scatter in the data.

The stress-strain curves for various moisture contents are shown in Figure 17 for four layer compaction specimen. The effects of a small amount of moisture are to increase the slope of the stress-strain curves, but continued increases in moisture content did not cause a continued increase in the slope of the stress-strain curves. This appears to be a result of an optimum moisture content, as discussed in Section IV.A.2. As in the case of the SHPB tests, the dry density of the static test specimen was held constant for all tests.

The static tests were conducted on a constant cross-head rate machine and displacement was calculated using a known time. This meant the unloading curve was not available, but observations of the load fall off, as the cross head speed was released, indicated an almost vertical slope.

SECTION V

CRITICAL INCIDENCE ANGLE STUDY

A. INTRODUCTION

As discussed in Appendix B, stress waves impinging on the interface between two media at incidence angles equal to or greater than the critical angle exhibit a characteristic much different than those which impinge at incident angles less than the critical incidence angle. Critical incident angles exist only when the incident stress wave is traveling in a medium which has a wave speed less than the corresponding wave speed in the refracted or transmitted medium. Therefore, the discussion of this section will be limited to longitudinal waves moving from a medium of lesser wave speed to that of a medium of greater wave speed. In this case, longitudinal waves are defined as waves having particle motions in the same direction as that of the wave front.

It can be shown analytically that at the critical angles, and greater, a wave is no longer refracted or transmitted in the normal manner but a refracted wave is established that travels along the interface of the two materials. The wave magnitude (displacement or stress) is shown to decay exponentially with distance from the interface, but it is not clear as to what magnitudes exist. These interface waves are discussed in some detail in Reference 17, and, for certain stiffness ratios and density ratios, these interface waves are propagated at wave speeds between the Rayleigh and transverse speed of the medium of greater density. These special waves are called Stonely waves (Reference 17) and their existence is limited to a very narrow range of material property ratios.

In other cases, where Stonely waves do not exist, the transmitted or refracted waves travel along the interface at the longitudinal and transverse speeds of the greater density material. The existence and use of the interface waves traveling at the higher longitudinal wave speeds are discussed in detail in Reference 7, relative to geologic refraction studies in earth layering. A case of this phenomenon for an interface between two solids is

52

given in Reference 17 for an incident medium of Plexiglas® bonded to a refractive medium of brass. The experiment for the Plexiglas®/brass interface shows the same general results as described for geologic refraction. However, no results were reported for stresses or strains in or near the interface.

B.   SIMPLIFIED ANALYSES

Some interesting results occur in the solutions of the reflected and transmitted ratios of Equations (B-6) and (B-8). In these analyses one must remember that these equations are based on elastic material response and that displacement continuity and stress equilibria must exist at the interface. Several wave speeds and densities were used in Equation (B-6) to show the effects of changes of wave speed and density for increasing incident angles. The various cases are shown in Table 6.

TABLE 6.   MATERIAL PROPERTIES FOR SIMPLIFIED ANALYSES

Case No.	Wave Speeds, km/sec				Density, kg/m^3	
	c_1	c_2	c'_1	c'_2	ρ	ρ'
1	5.0	3.0	5.0	3.0	1200	2400
2	5.0	3.0	5.0	3.0	2400	1200
3	5.0	3.0	2.5	1.5	2400	2400
4	2.5	1.5	5.0	3.0	2400	2400
5	0.68	0.43	3.4	2.1	1800	2400

For case 1, the wave speeds of the two materials making up the interface are the same, and a density ratio $\rho/\rho' = 0.5$. The results of these calculations are shown in Figure 21 where the ratio of the longitudinal transmitted wave to the longitudinal incident wave, σ_E/σ_A , is almost constant over the range of the incident angle α . For this same case, the reflected longitudinal stress ratio σ_C/σ_A is linearly decreasing with α and becomes negative at about $\alpha = 60^0$. For Case 2, the wave speeds are still constant, but the density ratio is increased and $\rho/\rho' = 2$. Again the transmitted stress ratio shown in Figure 22 is almost constant with α , but is approximately one-half that of Case 1. The reflected longitudinal stress

53

Figure 21. Transmitted/Refracted and Reflected
Longitudinal Stress Ratios Versus Incident
Angle for an Incident Longitudinal Stress σ_A.
Case 1 of Table 6.

54

Figure 22. Transmitted/Refracted and Reflected Longitudinal
Stress Ratios Versus Incident Angle for an
Incident Longitudinal Stress σ_A. Case 2 of Table 6.

55

ratio for this case is almost reverse that of Case 3, where it begins as negative and becomes positive at $\alpha = 60^0$. Since the wave speeds of the incident medium are equal to or greater than the wave speeds in the transmitted medium, there are no critical incidence angles for Cases 1, 2 and 3. For Case 3, the density ratio $\rho/\rho' = 1.0$ and the wave speeds in the incident medium are twice that of the wave speeds in the transmitted medium. The results for Case 3 are shown in Figure 23. If the wave speeds of Case 3 are reversed to give Case 4, then two critical incident angles exist

$$\alpha_{ci} = 28^? \text{ when } \eta = 90^0 \text{ and}$$
$$\alpha_{ct} = 56^0 \text{ when } \zeta = 90^0.$$

For the calculations involving critical incidence angles in Equation (8-6) the stress ratios are determined for incident angles α up to the critical angle α_{ci} at which time η is set to 90° and the calculations are continued until α_{ct} occurs, at which time ζ is set to 90° and calculations are continued to $\alpha = 90^?$. The results of Case 4 are shown in Figure 24 where discontinuities are shown at $\alpha = 28^0$ and $\alpha = 56^0$. The interesting results of Figure 24 are the high transmitted ratios obtained at angles slightly above α_{ci} and then a rather steep drop in the transmitted ratio down below zero (negative) to the next critical angle α_{ct}. This means that a possible sign change in the transmitted stress magnitude occurs at angles above the α_{ci} angle.

The ratio of the refracted characteristic impedance to the incident characteristic impedance of Case 5 is approximately 6.67 as compared to 2.0 of Case 4. However, in Case 5 the wave speed ratio is only 5.0, and this ratio controls the reflected and refracted angles through Snell's law. The results of Case 5 are shown in Figure 25. These critical incident angles appear to cause very little differences in the reflected ratios, but cause significant differences in the transmitted ratios.

Photoelastic studies of wave propagation are described in Reference 18, and additional studies of Reference 19 extended this work to include photoelastic analysis of wave propagation at interfaces of layered media. In Reference 19, photoelastic birefrigent materials were developed with longitudinal wave speeds in the ratio of approximately 2.0/1.0. Several
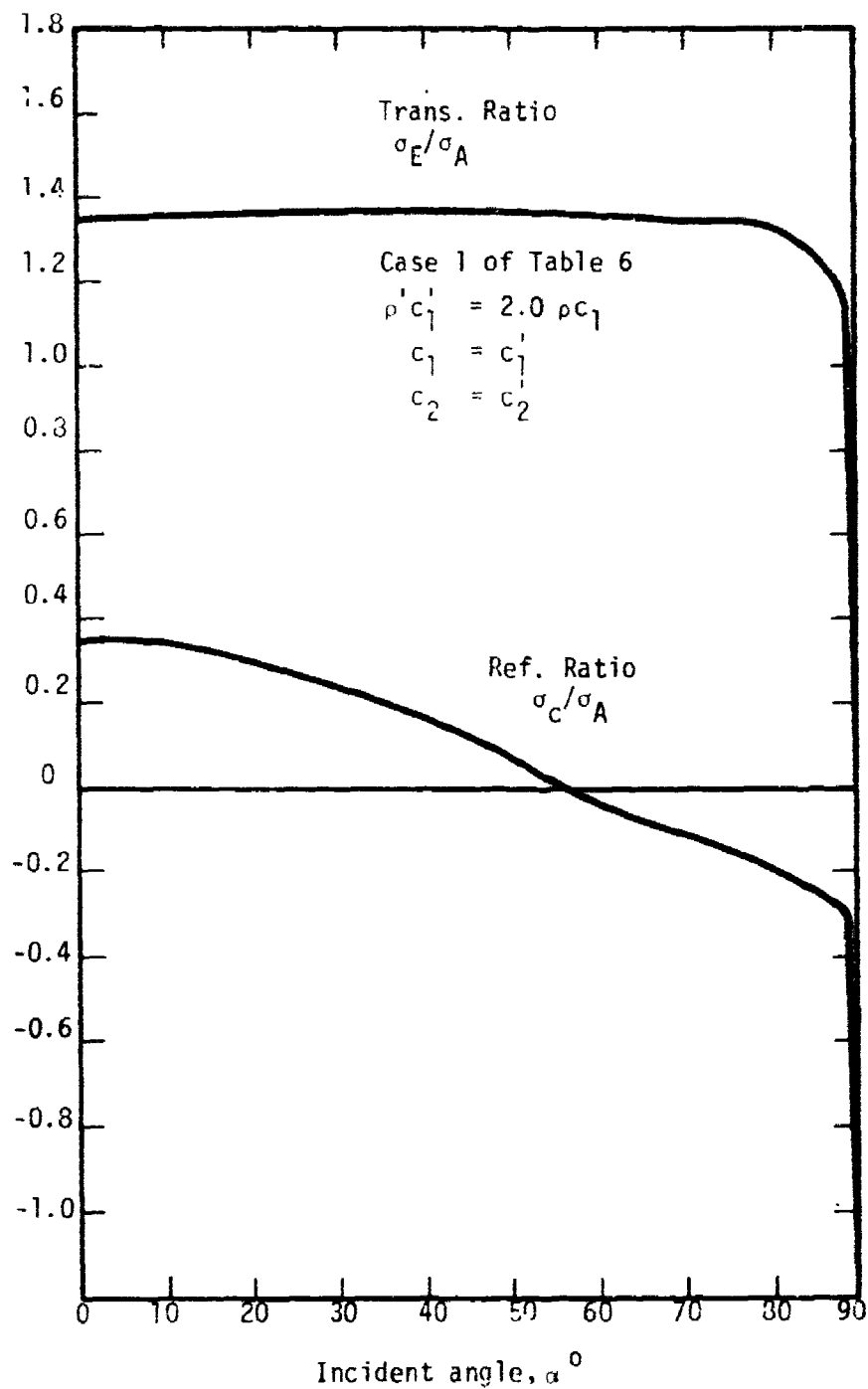
56

Figure 23. Transmitted/Refracted and Reflected Longitudinal Stress Ratios Versus Incident Angle for an Incident Longitudinal Stress σ_A. Case 3 of Table 6.
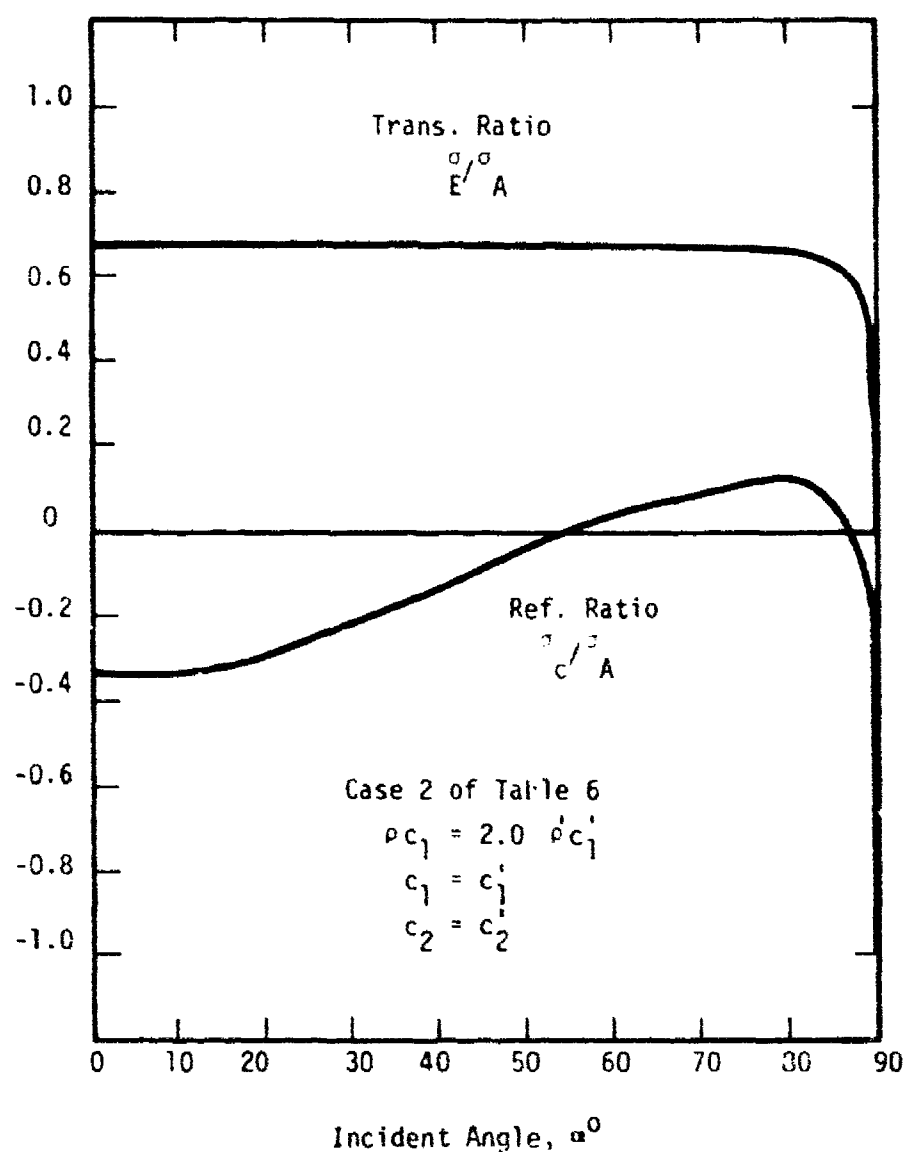
Figure 24. Transmitted/Refracted and Reflected Longitudinal Stress Ratios for an Incident Longitudinal Stress σ_A. Case 4 of Table 6.
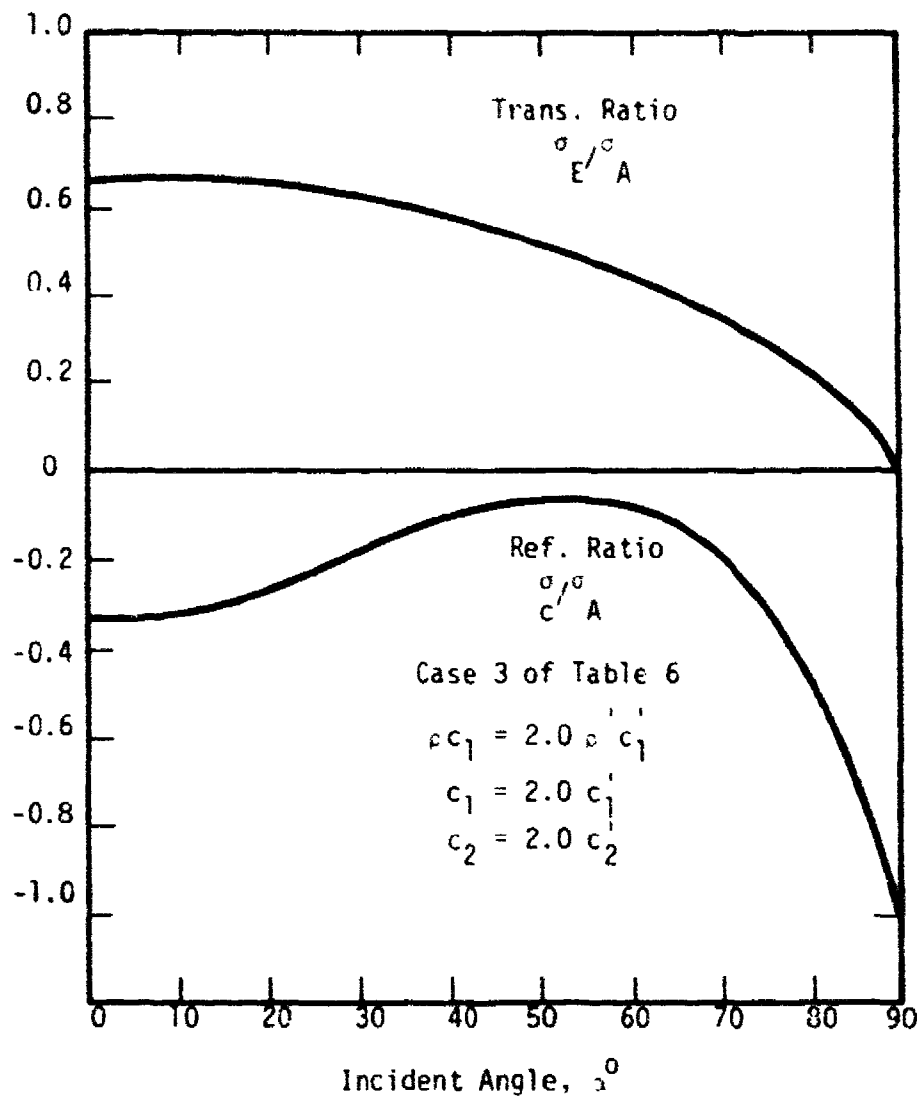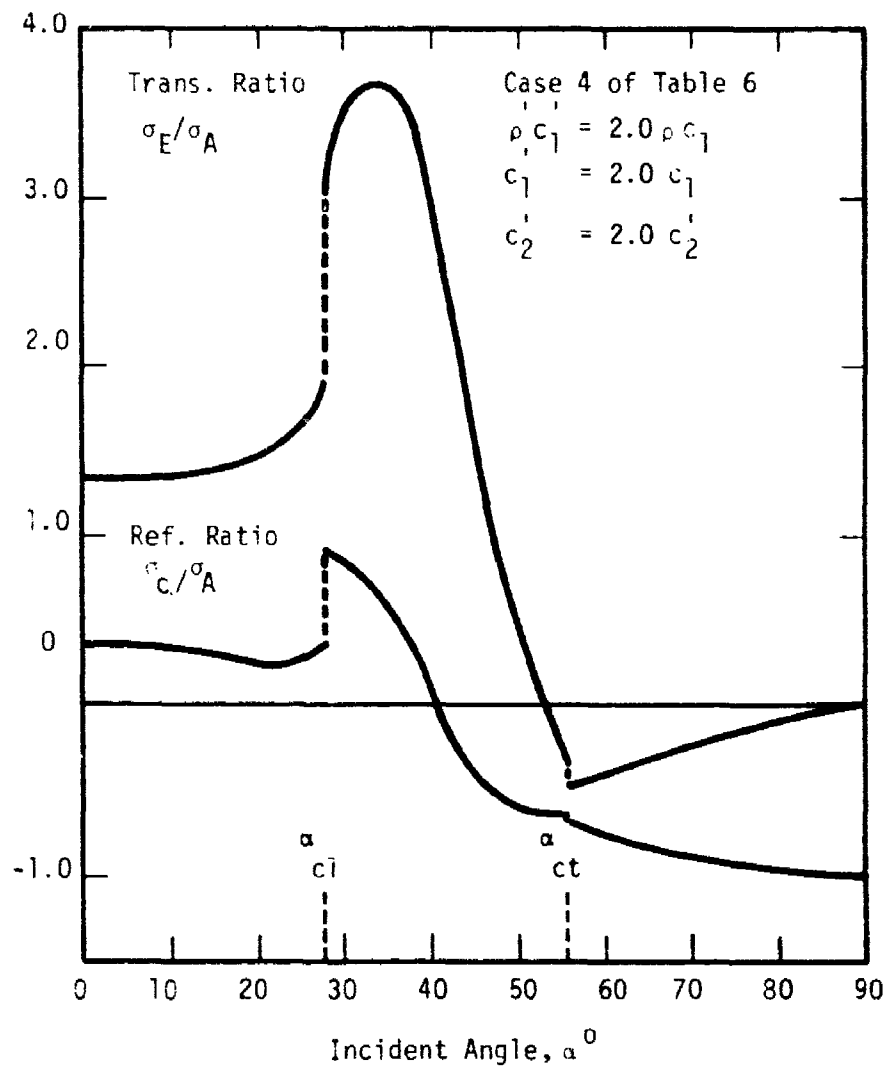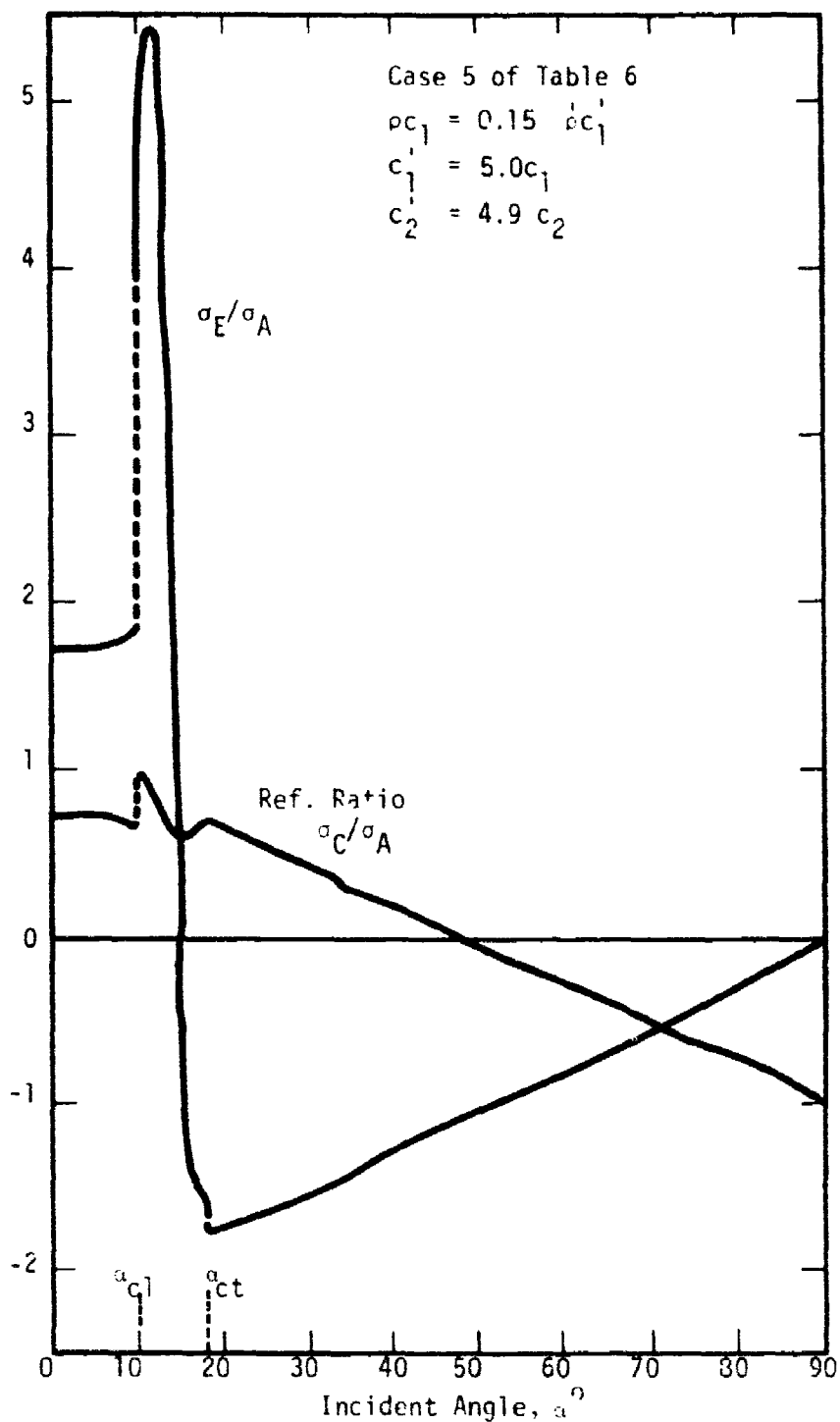
Figure 25. Transmitted/Refracted and Reflected Longitudinal Stress ratios Versus Incident Angle for an Incident Longitudinal Stress σ_A. Case 5 of Table 6.

experiments were conducted where a small charge was detonated in both the low wave speed material and in the higher wave speed material. Since the densities for both materials were the same, the ratio of wave speeds is equal to the ratio of characteristic impedances. If a pulse is propagating in the lesser wave speed material, regular reflection/refraction is in effect up to the first critical incidence angle α_{c1} . This phenomenon is shown schematically in Figure 26a. After this critical angle is exceeded, a refracted wave, denoted P_1P_2 in Figure 26b, runs out beyond the intersection of the incident pulse and the interface. This wave is a dilatation wave with two head waves, $P_1P_2P_1$ a dilational wave and $P_1P_2S_1$ a distortional wave, trailing behind in the incident medium. In addition, a distortional head wave $P_1P_2S_2$ trails behind P_1P_2 in the refracted medium. These waves are shown schematically in Figure 26 and were observed experimentally in Reference 19. A detailed discussion of these wave phenomena is found in References 17 and 19.

For one test of Reference 19 with the charge in the lesser wave speed medium an analysis was made for stresses along the interface in the greater wave speed medium. These stress levels as a function of time are shown in Figures 27 and 28. Some interesting results are worth pointing out. The stress σ_{yy} is compression within a small distance about twice the standoff (60°) beyond which σ_{yy} changes sign and is a tensile stress at the leading front of the wave. The σ_{xx} stress does not become compressive or have any significant stress value until about 1.5 times the standoff and stays compressive at the wave front beyond this value. Also, σ_{xx} of Figure 27 shows an increase in compressive stress, at the second time t_2, over the stress at time t_1.

In comparison, the refracted or transmitted stress of Figure 25 are a result of a wave speed ratio c_1'/c_1 of 2.0 similar to the results of Figures 25 and 26. This means the first critical incidence angle of Figure 25 is the same as for the data of Figures 27 and 28. For data of Figure 25, an increase in the refracted magnitude appears just beyond the first critical incidence and then falls and changes sign at approximately 50° (compression is positive in Figure 25 and negative in Figures 27 and 28). This same trend is evident in stresses of Figures 27 and 28. The analysis of Figure 24 is a plane wave

60

p   dilatational wave
S   shear wave
P_1 incident P wave
P_1P_1 reflected P wave
P_1S_1 reflected S wave
P_1P_2 refracted P wave
P_1S_2 refracted S wave

$P_1P_2P_1$ reflected P headwave
$P_1P_2S_1$ reflected S headwave
$P_1P_2S_2$ refracted S headwave
α incidence angle
α_{cl} critical dilatational incidence angle

(a) Wave positions before α_{cl}

(b) Wave positions after α_{cl}
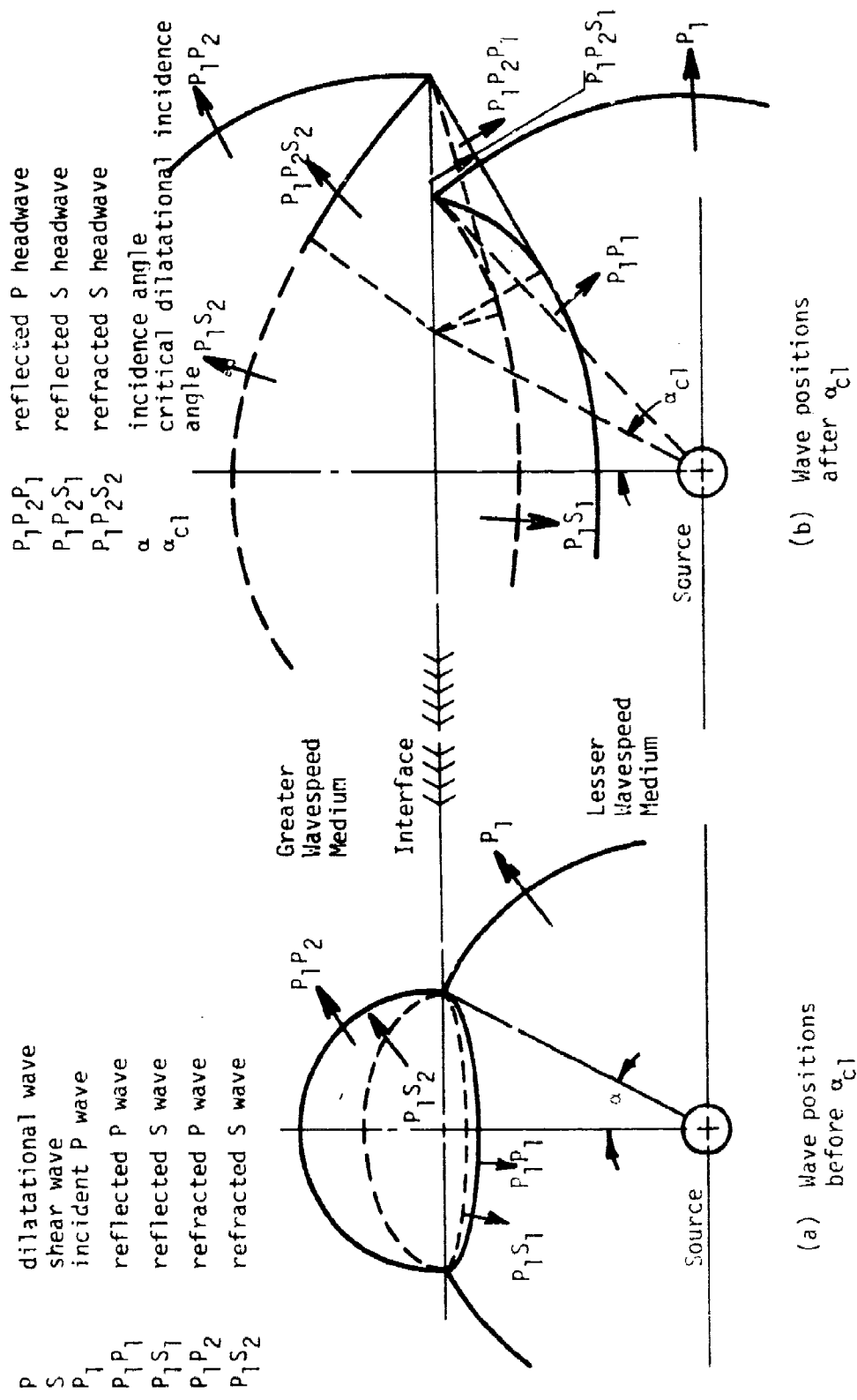
Figure 26. Sketch of Positions of Cylindrical Reflected and Refracted Waves as a Result of an Incident Cylindrical Dilatational Wave. (References 17 and 19).

61
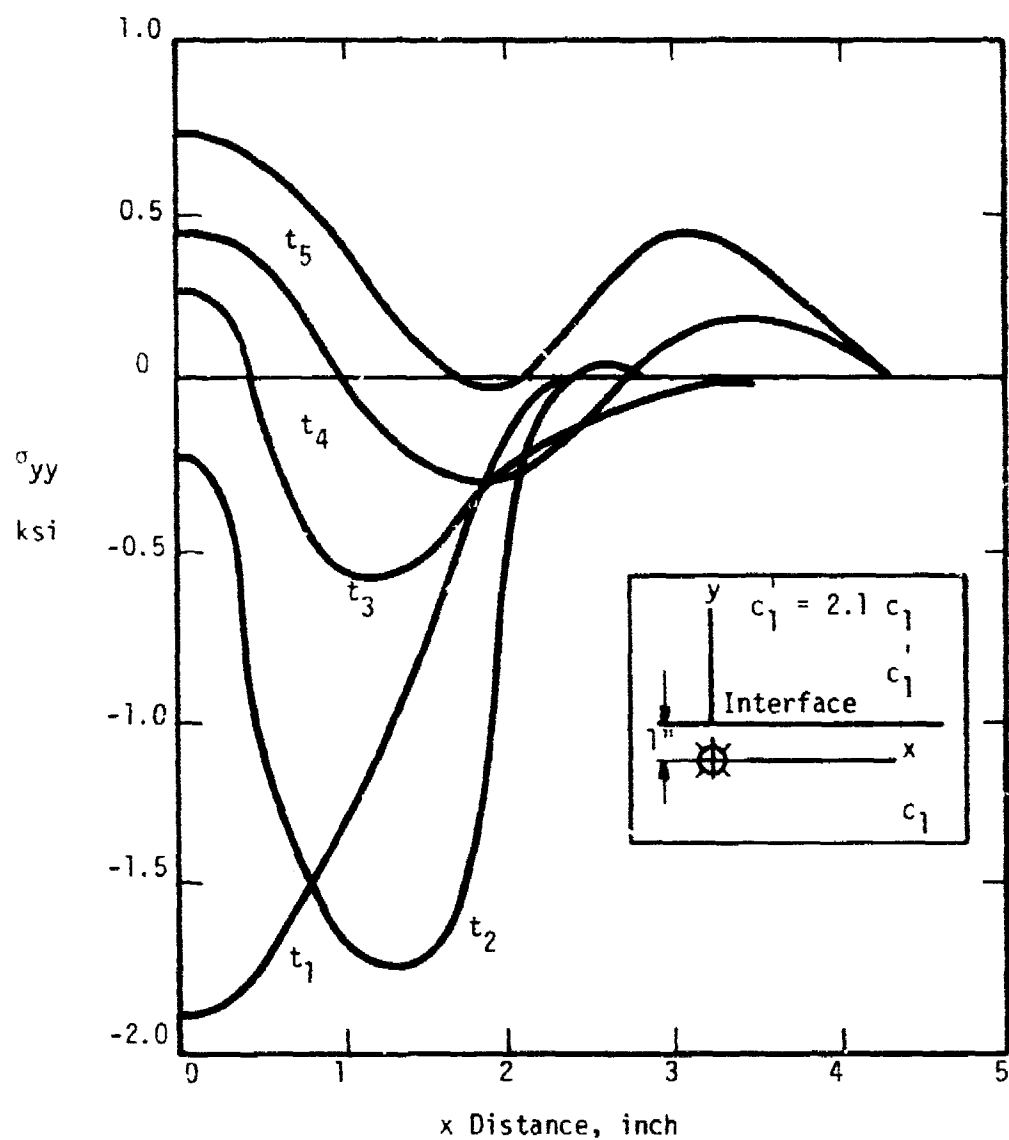
Figure 27. σ_{yy}, Stress Normal to Media Interface Versus Distance Along the Interface. Cylindrical Source in Lesser Wave Speed Medium (Results of Reference 19).
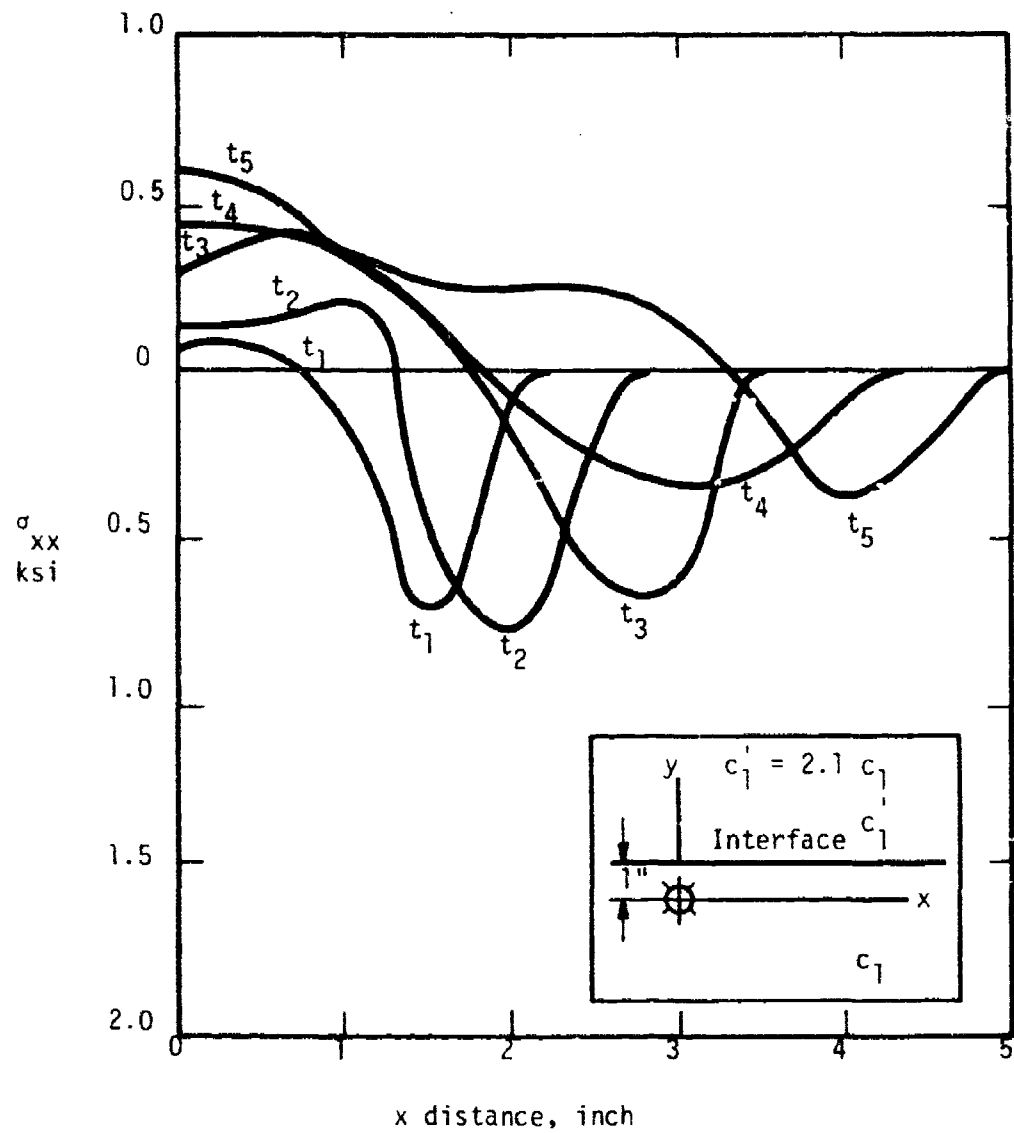
Figure 28. σ_{xx}, Stress Parallel to Media Interface Versus Distance Along the Interface Between Two Media Cylindrical Source in Lesser Wave Speed Medium. (Results of Reference 19).

63

solution, while the results of Figures 27 and 28 are from an experiment using
a cylindrical wave front. It is evident that qualitative results are similar.

SECTION VI

CONCLUSIONS AND RECOMMENDATIONS

A. CONCLUSIONS

The overall conclusion is that stress-strain curves, basic wave speed data, and material-damping coefficients along with effects of moisture content, gas content, and confining pressure may be obtained at intermediate strain rates in a split-Hopkinson pressure bar.

Based on the limited data obtained in this study the following general conclusions concerning split-Hopkinson bar tests are given:

1. For pressure waves with peak pressures between 300 and 1500 psi, the wave speeds of sandy soil are linear functions of confining pressure in the range of 0 to 300 psi.

2. For pressure waves with peak pressures between 300 and 1500 psi only slight decreases in damping coefficients of sandy soil are evident for confining pressure in the range of 0 to 300 psi.

3. For a given dry specimen density of sandy soil, increases in moisture content cause a significant decrease in damping coefficients and a slight increase in wave speed up to an optimum moisture content. Beyond the optimum moisture content, a decrease in wave speed and an increase in damping is experienced. If appreciable gas content is present, the wave speed stays depressed and material damping remains relatively high.

4. Specimen quality control is extremely important in both static and dynamic laboratory soil tests.

5. Scatter in the data of soils tests is to be expected for both laboratory tests and field tests.

6.   The effects of the "total reflection" phenomenon on the
     reflection/refraction of stress waves at interfaces are still
     unknown.

6.   RECOMMENDATIONS

1.   For future tests a specimen chamber similar to a static triaxial
     test cell should be installed in the split-Hopkinson pressure bar.
     This would allow for controlled degassing, addition of moisture, and
     confining pressure.

2.   Improve current strain gauge installation to allow for high input or
     incident stresses.

3.   Consider different bar material to eliminate the large mismatch in
     impedance between the bar and the soil. This would improve the
     reflection and transmission coefficients between the bar and the
     soil.

4.   Develop a better understanding of the wave propagation relative to
     "total reflection" phenomenon as well as explore applications to
     survivability/vulnerability problems.

66

REFERENCES

1. Westine, P. S. and Friesenhahn, G. J. Ground Shock Loads from Buried Combs and Ordnance Detonacions, AFATL-TR-82-19, Air Force Armament Laboratory, Eglin AFB, Florida, March 1982.

2. Summary Technical Report of Division 2, NDRC, Vol. 1. Effects of Impact and Explosion, National Defense Research Committee, J. B. Conant, Chairman, Division 2, E. B. Wilson Jr., Chief, Washington, D.C. 1946, AD 221 586.

3. A Manual for the Prediction of Blast and Fragment Loading on Structures DOE/TIC-11268, U. S. Department of Energy, Pantex Plant, Amarillo, Texas, November 1980.

4. Crawford, R. E., Higgins, C. J., and Bultmann, E. H., The Air Force Manual for Design and Analysis of Hardened Structures, AFWL-TR-74-102, Air Force Weapons Laboratory, Kirtland AFB, New Mexico, October 1974.

5. Merz, H. A., "A Survey of Models for Predicting the Ground Shock of Accidental Explosions in Underground Storage Facilities," Minutes of the Twentieth Explosives Safety Seminar, Volume II, Norfolk, Virginia, August 1982, pp 1309-1320.

6. Felice, C. W., Brown J. A., Gaffney, E. S., and Olsen, J. M., "An Investigation into the High Strain Rate Behavior of Compacted Sand Using the Split-Hopkinson Pressure Bar Technique," Proceedings of Second Symposium on the Interaction of Non-Nuclear Munitions With Structures, Panama City Beach, Florida, April 1985, pp 391-396.

7. Richart, F. E. Jr., Hall, J. R. Jr., and Woods, R. D., Vibrations of Soils and Foundations, Prentice-Hall Inc., Englewood Cliffs, New Jersey, 1970, pp 101-111.

8. Ross, C. A., "Dynamic Yield Stress of Metal Matrix Composites," Ph.D Dissertation, University of Florida, Gainesville, Florida 1971.

9.   ASME Boiler and Pressure Vessel Code Section VIII "Rules for
      Construction of Pressure Vessels," Div. 1, American Society of
      Mechanical Engineers, New York, New York, 1977 Edition.

10.   Love, A.E.H., A Treatise on The Mathematical Theory of Elasticity, Dover
      Publications New York, New York, 4th Edition 1944, p 287.

11.   Kolsky, H., Stress Waves in Solids Dover Publications, New York,
      New York 1964 p. 54.

12.   Follansbee, P. S. and Forantz, C., "Wave Propagation in the Split-
      Hopkinson Pressure Bar," J. of Eng. Mat. and Tech., Vol 105, Jan. 1983,
      pp 61-66.

13.   Hampton, D. and Wetzel, R. A., Stress Wave Propagation in Confined
      Soils, AFWL-TR- 66-56, Air Force Weapons Laboratory, Kirtland AFB, New
      Mexico, October 1966.

14.   Hall, J. R., Jr. and Richart, F. E., Jr., "Dissipation of Elastic Wave
      Energy in Granular Soils," J. of Soil Mech. and Found. Div. Proc. of
      ASCE, Vol 89, No. SM6, Nov. 1963, pp 27-55.

15.   Hardin, B. O. and Richart, F. E., Jr., "Elastic Wave Velocities in
      Granular Soils," J. of Soil Mech. and Found. Div., Proc. of ASCE Vol 89,
      No. SM1, February 1963, pp 33-64.

16.   Lambe, T. W. and Whitman, R. V., Soil Mechanics, J. Wiley and Sons, New
      York, New York, 1969.

17.   Ewing, W. M., Jardetzky, W. S., and Press, F., Elastic Waves in Layered
      Media, McGraw-Hill Book Co., New York, New York, 1957.

18.   Dally, J. W., and Riley, W. F., Photoelastic Study of Wave Propagation
      AFWL-TR-66-54, Air Force Weapons Laboratory, Kirtland AFB, New Mexico,
      October 1966.

19.   Daniel, I. M., <u>Photoelastic Study of Wave Propagation in Layered Media</u>, AFWL-TR-68-153, Air Force Weapons Laboratory, Kirtland AFB, New Mexico, July 1969.

20.   Lindholm, U. S., "Some Experiments with the Split Hopkinson Bar," <u>J. Mech. Phys. Solids</u> 12, 317, 1965.

21.   Sierakowski, R. L., Malvern, L. E., and Ross, C. A., <u>Compression Testing of Metals at Elevated Temperature</u>, AFATL-TR-80-76, Air Force Armament Lab., Eglin AFB, Florida, October 1981.

22.   Rinehart, J. S., <u>Stress Transients in Solids</u>, Hyperdynamics, Santa Fe, New Mexico 1975.

23.   MILHDBK-5, <u>Metallic Materials and Elements for Aerospace Vehicle Structure</u>, DOD, 1971.

24.   Jones, R. M., <u>Mechanics of Composite Materials</u>, McGraw Hill, New York, New York 1975.

25.   Charlie, W. A., Veyera, G. E., and Muzzy, M. W., "Shock Induced Soil Liquefaction Test Facility Development," 28th Int. Instrumentation Sym., ISA, Las Vegas, Nevada, May 1982.

APPENDIX A

SPLIT-HOPKINSON PRESSURE BAR

A. GENERAL DESCRIPTION

The compressive split-Hopkinson pressure bar uses the impact of one bar on another to generate a pressure wave and then uses this pressure wave to load a specimen sandwiched between two identical bars. A compressive split-Hopkinson pressure bar schematic is shown in Figure 1. Referring to Figure 1, the operation for a ductile metal specimen is as follows:

1. A striker bar is put in motion by a launcher and it impacts the incident bar with a velocity V.

2. The impact produces an almost rectangular stress pulse of magnitude $\rho c V/2$ in the striker bar and the incident bar. The pulse length in time is $t_s = 2L_s/c$; ρ is the striker bar length and c is wave speed.

3. The compressive stress pulse propagates away from the impacted ends of each bar at a speed of c. When the stress wave reaches the free end of the striker bar, it is completely reflected as a tensile wave and it travels back toward the impacted end. This tensile wave unloads the ends of the striker bar and the incident bar and the bars separate. The compressive stress returns to zero as the bars separate.

4. The compressive pulse travels down the incident bar and impinges on the sample sandwiched between the incident bar and the transmitter bar. Depending on the physical properties of the sample, portions of the stress pulse are reflected back into the incident bar and portions are transmitted into the transmitter bar. The reflected and transmitted portions of the stress pulse are proportional, respectively, to the strain and stress in the specimen.

70

5. Strain gages, located equidistant from tne specimen, provide time coincident pulses, which are used to measure the magnitude and duration of the incident, reflected and transmitted pulses. It can be shown (Reference 20-21) that the integral of the reflected pulse is proportional to the strain in the specimen and when displayed along with the transmitted pulse (proportional to stress in the specimen) a dynamic stress-strain curve can be determined.

Further details on principles of operation and description of the compression Hopkinson bar may be found in several publications such as References 20 and 21.

B.   EXPERIMENTAL CONSIDERATIONS FOR SOIL TESTS

It was proposed that controlled granular media and soil samples, encased in a hollow cylindrical sleeve that fits over each end of the incident and transmitter bar (see Figure 6), be placed in the specimen position of Figure 1. Also, a pressure transducer may be placed in the end of the transmitter bar next to the sample. Theoretically, one would know the details of the incident pressure pulse, based on measurements at the strain gage of the incident bar, as well as the details of the transmitted pulse from a strain gage placed on the transmitter bar. In addition, the pressure measurement from the transducer at the end of the soil specimen would be available for comparison. It is hoped that the presence of the pressure transducer will not alter the shape of the transmitted pulse. The bars with the transducer installed can be calibrated by simply wringing or pressing the bars together without a specimen. Usually small discontinuities in the bar do not cause problems in stress wave transmission. In fact, a tensile Hopkinson bar passes a compression pulse over the tensile specimen by use of a cylindrical tub: before the pulse is reflected from the far end of the bar and impinges on the specimen as a tensile pulse.

Using a constant impact bar velocity and resulting constant incident bar stress, specimen properties may be varied and their effects on the transmitted pressure magnitude and time duration may be evaluated. Tests can be run with

71

and without the transducer in place to determine the effects of the specimen properties on measurements made by the transducer.

Using this type of test device, the properties of the soil can be varied systematically to various stress levels by simply changing the striker bar velocity. Pulse duration can also be varied by changing the striker bar length. In addition, pulse shapes can be altered by introducing different types of buffer materials at the impact end of the incident bar. Finally, temperature control may be varied by installing a furnace, as was done in Reference 21, or placing a cooling device around the specimen. Corrections to the recorded strain readings must then be applied as given for example in Reference 21.

Questions concerning how much of the pressure pulse is transmitted to the soil sample and in turn how much of the stress pulse in the soil sample is transmitted to the transmitter bar may be approximated using one-dimensional elastic stress wave propagation. In the Hopkinson bar operation as described, the stress pulse transmission time across the specimen is so small when compared to the incident pulse length, that many reflections occur in the specimen while the incident pulse is traversing the specimen. Specimens whose acoustic impedance ρc were small in comparison to the acoustic impedance of the incident bar could not be tested to failure if it were not for the multiple reflections occurring. Returning to one-dimensional elastic wave propagation, when a wave is traveling in a medium of acoustic impedence $\rho_1 c_1$ and encounters an interface of another material of impedence $\rho_2 c_2$, the stress magnitude of the transmitted pulse σ_T and reflected pulse σ_R can be written in terms of the incident pulse σ_I . Using Figure A-1 and Reference 22 the following expressions may be found.

$$\frac{\sigma_R}{\sigma_I} = \frac{(\rho c)_2 - (\rho c)_1}{(\rho c)_1 + (\rho c)_2} \tag{A-1}$$

$$\frac{\sigma_T}{\sigma_I} = \frac{2(\rho c)_2}{(\rho c)_1 + (\rho c)_2} \tag{A-2}$$
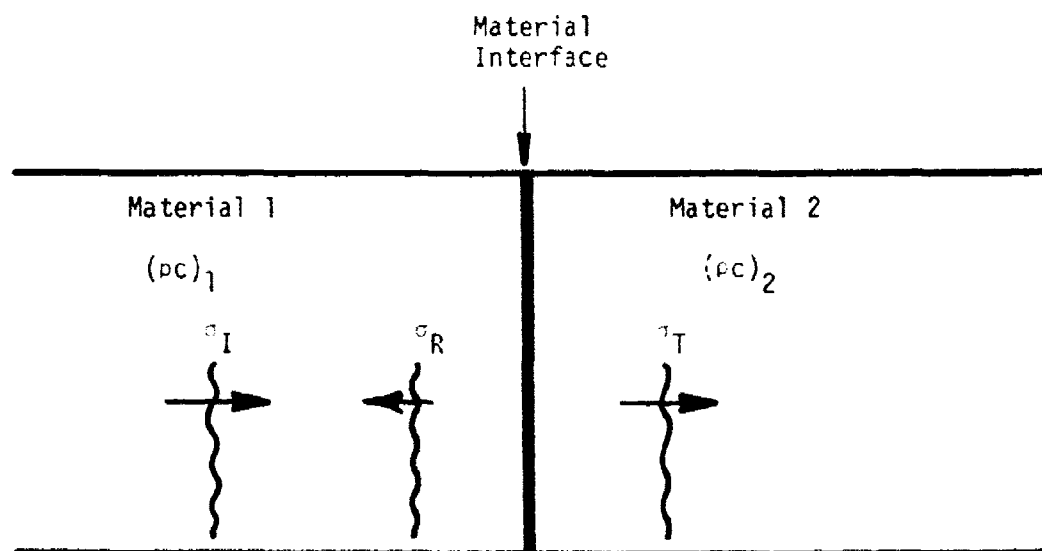
72

Figure A-1.   Schematic of an Interface.

If the two elastic materials go to infinity in both directions, a simple reflection and transmission take place, and this phenomenon may be treated as a simple stress wave propagation problem with the resulting reflected and transmitted wave forms almost completely independent of the incident length.

For the usual operation of the Hopkinson bar where dynamic properties of the specimen material are being sought, the incident pulse is many times longer than the specimen, and many reflections and transmissions will take place in the sample before the end of the incident pulse reaches the sample. This gives an almost equilibrium condition in the specimen before all portions of the incident pulse are completely transmitted or reflected. This means the sample would be loaded rather uniformly even though Equation (A-2) may show very small transmitted stresses if the acoustic impedance of the sample material is less than that of the incident bar material.

Tests using soil samples which are short compared to the length of the incident pulse may not give any indication of the transmissibility of the soil, but may, however, give an indication of the maximum load carrying capability of the soil type.

Test conditions where the incident pulse length is much shorter than the soil sample are a case of true wave propagation, and Equations (A-1) and (A-2) become important. Most Hopkinson bars are made of some type of steel which have approximate densities and elastic wave speeds of 7.84 g/cc and 5.08×10^5 cm/sec, respectively. If one were trying to load a sample of dry top soil which has an approximate density of 1.39 g/cc at an elastic wave speed of approximately 0.23×10^5 cm/sec, the transmitted pulse in the soil would be rather small for a steel incident bar. Typical ratios of σ_R/σ_I for a steel incident bar and a sandy soil sample are shown in Table A-1. Other incident bar materials having lower acoustic impedences than that of steel, such as titanium, aluminum, and glass/epoxy, might also be considered. The properties and stress ratios for these materials are shown in Table A-1 for three types of soil. Since the stress ratios are for a stress wave moving from the incident bar into the soil sample, σ_T would represent the transmitted pulse in the sample and σ_R would be the pulse reflected back into the incident bar.

74

TABLE A-1. MATERIAL PROPERTIES AND STRESS RATIOS

Material Properties

Material	Density, p g/cm^3	Wave Speed, c $(10^5)cm/sec$	p c $(10^5)g/cm^2/sec$
Sandy Top Soil (dry)*	1.39	0.23	0.32
Clayey Top Soil (dry)*	1.63	0.51	0.82
Clay (wet)*	1.99	1.37	2.73
Steel	7.84	5.08	39.83
Titanium	4.43	5.15	22.81
Aluminum	2.77	4.98	13.79
Glass/Epoxy	1.85	4.45	8.24
*Reference 23			

Stress Ratios

Incident Bar	Soil	s_T/s_I	s_R/s_I
Steel	Sandy	.02	.98
Steel	Clayey	.04	.96
Steel	Clay	.13	.87
Titanium	Sandy	.03	.97
Titanium	Clayey	.11	.89
Titanium	Clay	.21	.79
Aluminum	Sandy	.06	.94
Aluminum	Clayey	.11	.89
Aluminum	Clay	.33	.67
Glass/Epoxy	Sandy	.07	.93
Glass/Epoxy	Clayey	.18	.82
Glass/Epoxy	Clay	.31	.69

Based on Table A-1, the most promising incident bar materials appear to be aluminum and glass epoxy. The final selection would be based upon careful testing and screening of the candidate materials. Other types of materials, such as epoxy-impregnated wood, could also be used. As noted, the transmission ratios for soils are low, which may require high incident bar stress levels. However, the generated stress $\rho cV/2$ should not exceed the yield stress of the material. Returning to the candidate materials, extruded 7075 aluminum alloy has a yield strength of approximately 65,000 psi (0.45 GPa), Reference 23, while glass/epoxy composites are reported, as in Reference 24, to remain elastic up to essentially 150,000 psi (1.03 GPa). Thus, using the σ_T/σ_I ratios of Table A-1, there appears to be some question as to whether dry sandy soil could be loaded using some of the bar materials listed. However, a 100,000 psi pulse in a glass/epoxy incident bar could theoretically produce a 7,000 psi stress pulse in a sandy soil sample which would prove adequate for test purposes.

Looking at the pulse length requirement for a sandy soil sample, the travel time per centimeter is 1/c or about 44 μsec , using Table 1. In comparison, the travel time per centimeter for glass/epoxy is approximately 2.3 μsec . Based on these numbers, a 5 cm striker bar of glass epoxy would give a pulse length of 23 μsec and a 10 cm long soil sample would require 440 μsec for one pulse passage across the sample. These numbers would thus qualify as a meaningful wave propagation experiment.

Investigators of Reference 25 have resolved the problem of transmitting the pulse from the incident bar to the specimen by using a cylindrical incident bar filled with fluid, closed on one end by a piston, with a diaphragm separating the fluid from the specimen. However, the peak transmitted stress with this apparatus is limited to approximately 5000 psi (35 MPa). Variations of this method may prove to be a useful alternative scheme if solid incident bars prove to be totally unsatisfactory.

76

APPENDIX B

REFLECTION AND TRANSMISSION OF OBLIQUE INCIDENT ELASTIC
STRESS WAVES AT AN INTERFACE BETWEEN TWO SOLIDS

A. INTRODUCTION

In general, when an incident longitudinal stress wave impinges on an interface between two elastic solids, both longitudinal and transverse waves are reflected and transmitted. This section is restricted to the discussion of the reflected and transmitted planar longitudinal waves. A general schematic of a longitudinal incident wave/interface interaction is given in Figure B-1. The following nomenclature is associated with the longitudinal incident planar wave of Figure B-1.

B. NOMENCLATURE

A, σ_A Incident Longitudinal Displacement and Stress at Angle α

C, σ_C Reflected Longitudinal Displacement and Stress at Angle α

D, σ_D Reflected Transverse Displacement and Stress at Angle β

E, σ_E Transmitted Longitudinal Displacement and Stress at Angle η

F, σ_F Transmitted Transverse Displacement and Stress at Angle ζ

C_1, C_2, ρ Incident Longitudinal, Transverse Wave Speeds and Density

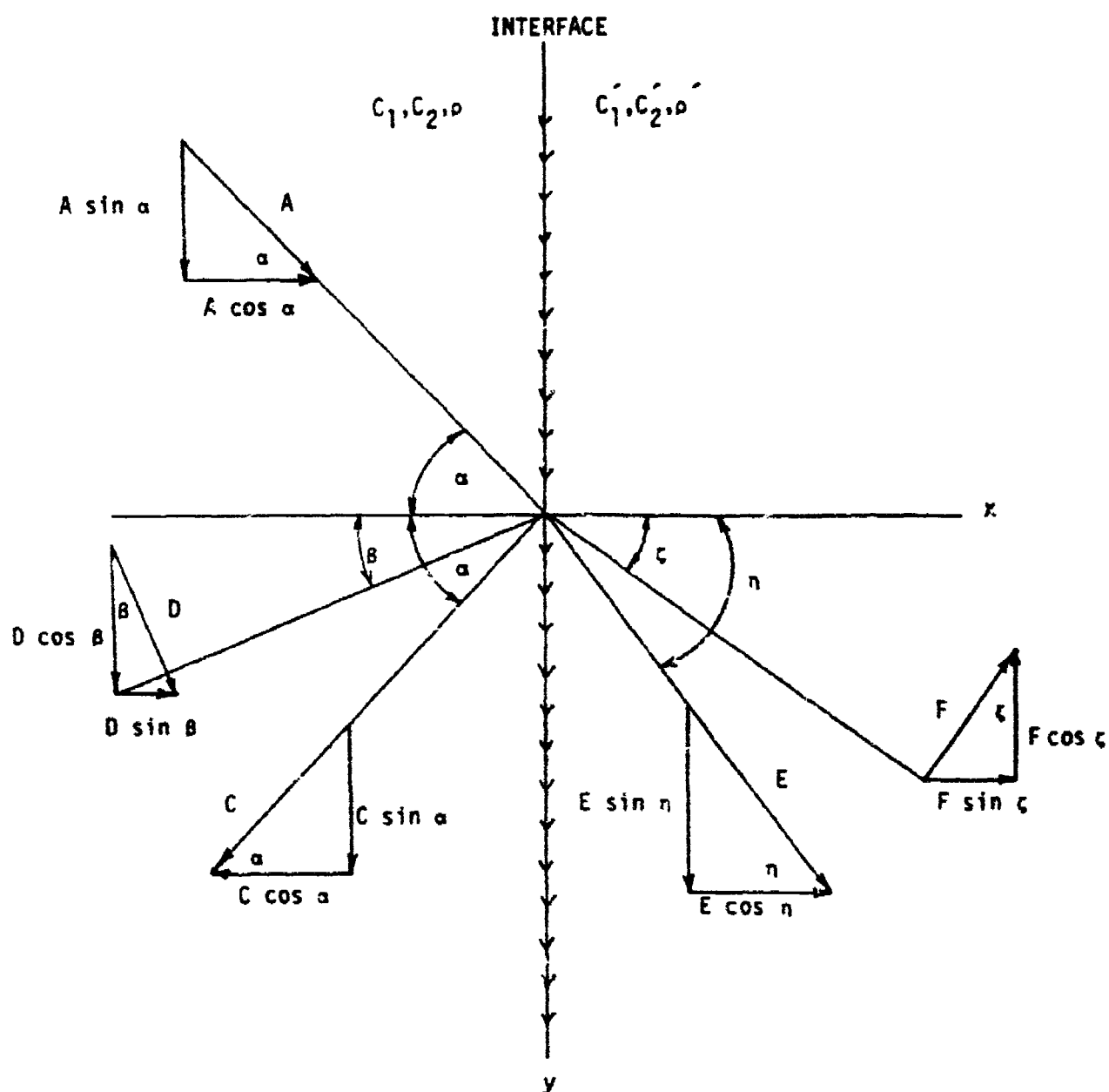C_1', C_2', ρ' Transmitted Longitudinal, Transverse Wave Speeds and Density

Figure B-1. Displacement Schematic for an Incident
Longitudinal Wave A.

C. BOUNDARY EFFECTS ON ELASTIC WAVE PROPAGATION

Equations relating the displacements A, C, D, E, F of Figure B-1 may be written using the interface boundary conditions of Equation (B-1), equal normal displacements across the interface, Equation (B-2), equal tangential displacements across the interface, Equation (B-3), equal normal stresses across the interface, and Equation (B-4), equal tangential stresses across the interface. These general interface boundary conditions for motion in the xy plane are given in Reference 11 as

$$\Sigma u = \Sigma u' \tag{B-1}$$

$$\Sigma v = \Sigma v' \tag{B-2}$$

$$\Sigma \sigma_{xx} = \Sigma \sigma'_{xx} \tag{B-3}$$

$$\Sigma \left[(\lambda + 2\mu)\frac{\partial u}{\partial x} + \lambda\frac{\partial v}{\partial y} \right] = \Sigma \left[(\lambda+2\mu)\frac{\partial u}{\partial x} + \lambda\frac{\partial v}{\partial y} \right]'$$

$$\Sigma \sigma_{xy} = \Sigma \sigma'_{xy} \tag{B-4}$$

$$\Sigma \left[\mu \frac{\partial u}{\partial y} + \frac{\partial v}{\partial x} \right] = \Sigma \left[\mu \frac{\partial u}{\partial y} + \frac{\partial v}{\partial x} \right]'$$

where u, v = x, y displacements

μ, λ = Lame's constants

σ_{xx}, σ_{xy} = Normal, Tangential Stresses

79

and the unprimed and prime terms are associated with the left and right, respectively, of the interface of Figure B-1. The general displacement for a simple harmonic wave is given as

$$u_i = \phi_i \cos\theta_i$$

$$v_i = \phi_i \sin\theta_i \qquad (B-5)$$

$$\phi_i = U_i \quad \sin(pt) + \frac{p}{C_i}(\cos\theta_i)x + \frac{p}{C_i}(\sin\theta_i)y$$

where

$$U_i = A, C, D, E, F$$

$$\theta_i = \alpha, \beta, \zeta, \eta$$

$$p = \text{frequency}$$

$$C_i = C_1, C_2, C_1', C_2'$$

The equations relating A,C,D,E,F are given in Reference 22

$$A\cos\alpha - C\cos\alpha + D\sin\beta - E\cos\eta - F\sin\zeta = 0$$

$$A\sin\alpha + C\sin\alpha + D\cos\beta - E\sin\eta - F\cos\zeta = 0$$

$$A\cos2\beta + C\cos2\beta - D(C_2/C_1)\sin2\beta - E(\rho'/\rho)(C_1'/C_1)\cos 2\zeta - \qquad (B-6)$$
$$F(\rho'/\rho)(C_2'/C_1)\sin 2\zeta = 0$$

$$A\sin2\alpha - C\sin2\alpha - C(C_1/C_2)\cos2\beta - E(\rho'/\rho)(C_2'/C_2)^2(C_1/C_1')\sin2\eta +$$
$$F(\rho'/\rho)(C_2'/C_2)^2(C_1/C_1')\cos2\zeta = 0$$

80

In addition, Snell's law must be imposed and

$$(\sin a)/C_1 = (\sin B)/C_2 = (\sin n)/C_1' = (\sin \zeta)/C_2' \qquad (B-7)$$

Equation (B-5) may be cast in matrix form, shown in detail in Reference 22 and solutions produce displacement ratios C/A, D/A, E/A and F/A, assuming Equations B-6 are valid. The stress ratios are related to the displacement ratios through characteristic impedence ratios. It may be shown that

$$\frac{C}{A} = \frac{\sigma_C}{\sigma_A}, \quad \left(\frac{C_1'}{C_1}\right)\frac{D}{A} = \frac{\sigma_D}{\sigma_A} \qquad (B-8)$$

$$\left(\frac{\rho'C_1'}{\rho\, C_1}\right)\frac{E}{A} = \frac{\sigma_E}{\sigma_A}, \quad \left(\frac{\rho'C'_2}{\rho\, C_1}\right)\frac{F}{A} = \frac{\sigma_F}{\sigma_A}$$

The above relationships are easily checked by using an example of normal incidence i.e., $a = B = n = \zeta = 0$ in Equation (B-6). The normal incidence of a longitudinal wave results only in reflected and transmitted longitudinal waves. The resulting nonzero displacement ratios for normal incidence of Equation (B-6) are

$$\text{Reflected Ratio} \quad \frac{C}{A} = \frac{\rho'C_1' - \rho C_1}{\rho C_1 + \rho'C_1'}$$

$$\text{Transmitted Ratio} \quad \frac{E}{A} = \frac{2\,\rho C_1}{\rho C_1 + \rho'C_1'} \qquad (B-9)$$

Using Equations (B-8) and (B-9), the stress ratios for normal incidence are

$$\frac{\sigma_C}{\sigma_A} = \frac{\rho'C_1' - \rho C_1}{\rho C_1 + \rho'C_1'} \qquad (B-10)$$

$$\frac{\sigma_E}{\sigma_A} = \frac{2\,\rho'C_1'}{\rho C_1 + \rho'C_1'}$$

81

Note that only a change occurs for the transmitted ratio. The above Equations (B-9) and (B-10) are valid only for normal incidence and Equation B-6 is automatically satisfied for $\alpha = 0$. For angles other than $\alpha = 0$, Equation (B-4) must also hold, and for the case of wave speeds in the incident or unprimed medium less than those of the prime or transmitted medium, the angles η and ζ approach $\pi/2$. This phenomenon in optics is referred to as "total reflection" and theoretically no waves are transmitted or refracted into the primed medium. This means there are two critical incidence angles

$$\alpha_{ci} = \sin^{-1}\left(\frac{c_1}{c'_1}\right) \tag{B-11}$$

for $\sin \eta = 1$

and

$$\alpha_{ct} = \sin^{-1}\left(\frac{c_1}{c'_2}\right) \tag{B-12}$$

for $\sin \zeta = 1$.

For a planar wave with an incident angle of Equation (B-11), no longitudinal wave is refracted or transmitted and for Equation (B-12), no transverse wave is refracted or transmitted. In most materials the shear or transverse wave speed is less than the longitudinal wave speed which indicates that, for increasing angles of α, η would approach $\pi/2$ prior to that of the angle ζ. Using this same assumption, then β would always be less than α. Experimental evidence indicates that total reflection does exist at air/prism interfaces in optics, thermal layering in large bodies of water, and layering of soils having different wave speeds. There appears to be very little experimental evidence of total reflection at interfaces of two solids or a rather soft/hard interface such as a soil/concrete interface.

The phenomenon of total reflection still holds for spherical or cylindrical waves; however, the interaction of these waves with the interface

82

cylindrical waves; however, the interaction of these waves with the interface is very complicated and some discussion of a cylindrical wave interacting with an interface between two dissimiliar media is included in Section V.B.